31 de enero, 2017

Reporte de la utilización, avances y productos obtenidos
Dr. Carlos Amador Bedolla
Facultad de Química, UNAM

1. Título(s)

En el año de 2016, el grupo de trabajo que dirijo utilizó los recursos de supercómputo en los proyectos que se mencionan a continuación.

Proyecto 1: Estudio de propiedades electrónicas de compuestos orgánicos para su empleo en celdas fotovoltaicas y baterías de flujo. Carlos Amador Bedolla
Proyecto 2: Estudio teórico experimental del fenómeno de entrecruzamiento de espín en compuestos de Fe(III) con el ligante bztpen. Martha Magdalena Flores Leonar
Proyecto 3: Estudio teórico-experimental de los componentes de una celda fotovoltaica de unión líquida con pigmentos adsorbidos. Paulino Guillermo Zerón Espinosa.
Proyecto 5: Evaluación de Funcionales de la Densidad en el estudio de estructuras supramoleculares. Nancy Cihuapilli Barrueta Flores
Proyecto 6: Transferencia de carga en oligómeros con potencial como celdas fotovoltaicas. Gerardo Alvarez Alvarez (Maestría, fecha estimada de obtención del grado, junio 2017)

2. Resumen

Los proyectos presentados y desarrollados durante 2016 han sido integrados en el en el Proyecto de Investigación Grande que se presenta en esta convocatoria. Este proyecto (con financiamiento de CONACyT-SENER) ha permitido el crecimiento considerable del grupo de trabajo ---de cinco a nueve miembros--- que solicita recursos de supercómputo. Los miembros de este grupo tienen amplia experiencia en el uso de supercómputo, sea por su participación pasada en este grupo o por su adición a éste luego de participar en otros proyectos. El proyecto integrado presente continua con los objetivos fundamentales de los proyectos individuales presentados en 2016.

3. Breve descripción de avances

Proyecto 1. Elaboramos una modificación de la teoría de Marcus para predecir la

rapidez de reacción para la transferencia de excitones en moléculas orgánicas donador y aceptor. El avance de esta etapa del proyecto es de 80%. Escribimos un reporte preliminar que anexamos (Anexo 1). No ha sido enviado a publicación, pero se espera hacerlo en breve.
Proyecto 2: El estudio teórico de la totalidad de este proyecto ha sido prácticamente terminado. El principal resultado de este proyecto es la graduación de la estudiante de doctorado, previsto para junio de este año. El artículo mencionado en la solicitud ha sido publicado (Anexo 2). Otro artículo con resultados de este año ha sido enviado para su revisión y posible publicación (Anexo 3) .
Proyecto 3: Los avances de este proyecto, que a la fecha son de 90% del total estimado, han permitido la realización de un subproyecto de cómputo relacionado que muestran avance, por su parte, de 70%. Este subproyecto se realiza en colaboración con un posdoctorante de la UAM-I para quien se pidió una cuenta adicional (Javier Carmona Espíndola). Dos artículos de investigación se encuentran en elaboración y se espera su publicación en este año.
Proyecto 5: La estudiante presentó y aprobó su examen de grado de licenciatura en donde incluyó resultados de cálculos realizados con los recursos de supercómputo (Anexo 4). El proyecto se considera terminado. Este año, con base en las experiencias obtenidas, aplicará este tipo de estudios a moléculas orgánicas fotovoltaicas como parte de sus estudios de maestría que permitirán su graduación en agosto de 2018.
Proyecto 6: El proyecto muestra un avance de 60%. Su principal producto será la tesis de maestría del estudiante que obtendrá el grado correspondiente en agosto de 2017.

4. Cálculos realizados

Se realizaron cálculos de optimización de estados basales para numerosos sistemas ---orgánicos y con metales de transición--- en fase gas y en PCM con las suites Gaussian y QChem y el empleo de diversos funcionales dentro de DFT. De la misma manera se realizaron cálculos de optimización de estados excitados con TDDFT. Adicionalmente se llevaron a cabo cálculos de mecánica molecular con Amber-16 para sistemas extensos de moléculas orgánicas.

5. Software utilizado

- QChem 4.3
- Gaussian09
- Amber16

6. Recursos utilizados

636,289 horas de CPU
Ver detalle en el Anexo 5. Detalle de Consumo

7. Lista de colaboradores

1. Carlos Amador Bedolla
2. Martha Magdalena Flores Leonar (alumna de Doctorado)
3. Gerardo Álvarez Álvarez (alumno de Maestría)
4. Nancy Cihuapilli Barrueta Flores (alumna de Maestría)
5. Javier Carmona Espíndola (colaborador, posdoctorado UAM-I, inició colaboración empleando Miztli en diciembre, 2016)
6. Paulino Guillermo Zerón Espinosa (colaborador, estudiante de doctorado FQUNAM)

Los colaboradores mencionados en la lista anterior son quienes emplearon directamente los recursos de supercómputo. Los colaboradores en el proyecto incluyen también a:

Víctor Ugalde Saldívar (FQ-UNAM)
Rafael Moreno Esparza (FQ-UNAM)
Laura Domínguez Dueñas (FQ-UNAM)
Ignacio González Martínez (UAM-I)
José Luis Gázquez Mateos (UAM-I)

8. Lista de artículos publicados.

1. Further insights in DFT calculations of redox potential for iron complexes: the ferrocenium/ferrocene system
   Martha M. Flores-Leonar, Rafael Moreno-Esparza, Víctor M. Ugalde-Saldívar and Carlos Amador-Bedolla
   Computational and Theoretical Chemistry 1099C (2017) pp. 167-173
   http://dx.doi.org/10.1016/j.comptc.2016.11.023
2. (Enviado) GPU Algorithm for the Scaled Opposite-Spin (SOS) MP2 Energy Evaluation
   Luis Ángel Martínez-Martínez and Carlos Amador-Bedolla
   Submitted for publication to Journal of the Mexican Chemical Society (05.09.16)
3. (Enviado) Correlating properties in iron(III) complexes: A DFT description of structure, redox potential and spin crossover phenomena
   Martha M. Flores-Leonar, Rafael Moreno-Esparza, Víctor M. Ugalde-Saldívar and Carlos Amador-Bedolla
   Submitted for publication to Chemistry: A European Journal (12.16)

9. Lista de alumnos graduados.

1. Nancy Cihuapilli Barrueta Flores. Química, Facultad de Química, UNAM. *Evaluación de funcionales de la densidad en el estudio de estructuras supramoleculares*. 23 de septiembre de 2016. Aprobada con mención honorífica.

10. Lista de congresos nacionales e internacionales y participantes.

2. Conferencia “Fotovoltaicas Orgánicas: De la predicción a la síntesis”. 51° Congreso Mexicano de Química, Simposio 5: Síntesis de materiales para la producción y almacenamiento de energía. Pachuca, Hgo. 30 de septiembre, 2016. (Con José Alfredo Vázquez Martínez)
3. Póster. “Transferencia de carga en sólidos amorfos orgánicos: geometría intra e intermolecular". Semana de la Investigación, Facultad de Química, UNAM, 13-14 de octubre 2016. Con Nancy Cihuapilli Barrueta Flores, Augusto González Navejas, Karl García, Gerardo Álvarez Álvarez, Brenda Vargas Rocha y Martha M. Flores Leonar.
4. Presentación oral. “Teoría de Marcus para superficies de potencial con curvaturas diferentes”. XV RMFQT. Mérida Yucatán 17-19 de noviembre 2016. Con Brenda Vargas Rocha.
5. Póster. “Geometría de estados excitados en confórmeros OPV”. XV RMFQT. Mérida Yucatán 17-19 de noviembre 2016. Con Gerardo Álvarez Álvarez.
6. Póster. “Predicción de las estructuras supramoleculares en la interfase de OPVs: moléculas orgánicas pequeñas con PCBM”. XV RMFQT. Mérida Yucatán 17-19 de noviembre 2016. Con Nancy Cihuapilli Barrueta Flores.
7. Póster. “Dinámica molecular de la fase donadora de heterojuntas de fotovoltaicas orgánicas. XV RMFQT”. Mérida Yucatán 17-19 de noviembre 2016. Con Augusto González-Navejas, Karl García, Laura Domínguez.
8. Póster. “Comportamiento sistemático de funcionales de la densidad en la predicción del espectro electrónico del pigmento Ru535 utilizando TDDFT”. XV RMFQT. Mérida Yucatán 17-19 de noviembre 2016. Con Paulino Zerón, Javier Carmona Morales, Martha M. Flores Leonar, José Luis Gázquez Martínez, Ignacio González, Víctor Manuel Ugalde Saldívar.
9. Conferencia “The Clean Energy Project: from Prediction to Synthesis” NANOMXCN-2016, City University of Hong Kong. Mexico-China Workshop on Nano: Materials / Science / Technology, Renewable Energy and Environmental Remediation. 04-06 December, 2016 (Su-Tu)

Marcus theory for potential surfaces with different curvature

Carlos Amador-Bedolla[a,*], Brenda Vargas-Rocha[a]

[a] *Facultad de Química, Universidad Nacional Autónoma de México, México D.F. 04510, México*

Abstract

Marcus theory of electron transfer assumes that potential surfaces of reactants and products are parabolic and have the same curvature. Even though this is not generally the case, Marcus theory has been successful in predicting reaction rates in a wide variety of chemical reactions. An extension to Marcus theory in which potential surfaces, while still parabolic, are allowed to have different curvatures is offered in this paper. As an example of the effects of this modification, this procedure is applied to molecules proposed for exciton and charge transfer in OPVs, where we observe considerable differences in the predicted transition Gibbs energies by a factor of two.

Keywords: Marcus theory, exciton and charge transfer, OPVs

---

1. Introduction

In a chemical reaction [1], reactants, originally in the minimum of the potential energy surface, will react following a complex reaction coordinate, always climbing through the potential energy surface until they reach a (multidimensional) saddle point where they will begin their descent, still through the reaction coordinate on top of the potential energy surface of the products. Marcus theory provides a way of calculating the energy of the saddle point where the two potential energy surfaces (the one for the reactants and the one for the products) intersect. This intersection point occurs someplace over the reaction coordinate and corresponds to a particular rearrangement of the

---

[*] Corresponding author

Email address: `carlos.amador@unam.mx` (Carlos Amador-Bedolla)

reactants. Interestingly, in Marcus formulation, by assuming equal curvatures for the potential energy surfaces, this unknown intermediate structure is not needed and in order to calculate its energy value it is only necessary to calculate the value of the potential energy of products at the structure of the reactants. In the next section we remind of the deduction of this very well known result.

2. Marcus theory

Let us start with an exciton transfer reaction for a donor molecule, D, in the donor region of a heterojunction organic photovoltaic to an acceptor molecule, A, in the acceptor region. The reaction is assumed to be

$$D^* + A \rightarrow D + A^* \tag{1}$$

Where D^* is an excited molecule —carrying an exciton— and A is an acceptor molecule in its basal state. D^* will transfer its exciton to A ending up in the basal state, D, and exciting the second molecule to A^*.

We assume a parabolic potential for the reactant molecular pair and an identical parabolic potential for the product molecular pair. We follow the potential over a reaction coordinate. This situation is represented in Figure 3. The minimum of the potential curve for the reactants is $G_1^0 = G_{D^*}^0 + G_A^0$ and is located at a reaction coordinate of x_1, while the minimum for the potential curve of the products is $G_2^0 = G_D^0 + G_{A^*}^0$ and is located at reaction coordinate x_2. Equation for each parabolic potential is

$$\begin{aligned} G_1(x) &= G_1^0 + k(x - x_1)^2 \\ G_2(x) &= G_2^0 + k(x - x_2)^2 \end{aligned}$$

Solving for x_I that makes $G_1(x_I) = G_2(x_I)$, the value of the potential energy at the intersection is

$$G_1(x_I) = G_1^0 + \frac{(\Delta G^0 + k(x_2 - x_1)^2)^2}{4k(x_2 - x_1)^2}$$

Or, as it is commonly expressed in terms of the transition state energy,

$$\begin{aligned} \Delta G^\dagger &= G_1(x_T) - G_1^0 \\ &= \frac{(\Delta G^0 + \lambda)^2}{4\lambda} \end{aligned} \tag{2}$$

Where $\lambda = k(x_2 - x_1)^2$ is the reorganization energy. Notice that the transition state energy calculation does not require knowledge of the reaction coordinate as it depends only on its value at the structure of the minimum of reactants and of the structure at the minimum of products. Notice further that, because the curvature of the parabolas is the same, one need only know the structure of one minimum point —either reactants or products—. In our example, the reorganization energy can be evaluated as

$$G_2(x_1) - G_1(x_1) = G_2(x_1) - G_1^0 = \lambda + \Delta G$$

or as

$$G_1(x_2) - G_2(x_2) = G_1(x_2) - G_2^0 = \lambda - \Delta G$$

The fortunate transformation of the required quantities to only include $k(x_1 - x_2)^2$ has allowed Marcus theory to be easily applicable to a wide variety of situations and have also provided important results [2, 3].

In one of the original papers by Marcus, an extension of this theory for the case of asymmetrical parabolas was considered [4]. Recently, this idea has been applied to the study of electrode processes for the estimation of oxidation and reduction rate constants [5, 6]. The approximation suggested in this paper applies easily to a general charge transfer reaction.

3. Transition state energy for $k_1 \sim k_2$

If the curvature of the two parabolas is not the same, the value of the reaction coordinate for the intersect is given by

$$(k_2 - k_1)x^2 - 2(k_2x_2 - k_1x_1)x + \left(G_2^0 - G_1^0 + k(x_2^2 - x_1^2)\right) = 0$$

For $k_2 \sim k_1$, this equation can be solved approximately by

$$x = \frac{\Delta G^0 + k_2x_2^2 - k_1x_1^2}{2(k_2x_2 - k_1x_1)},$$

and the transition state energy is given by

$$\Delta G^\dagger = k_1\left(\frac{\Delta G^0 + k_2x_2^2 - k_1x_1^2}{2(k_2x_2 - k_1x_1)}\right)^2 \qquad (3)$$

This expression can no longer be calculated by the energy difference between the two surfaces at the reactants or products reaction coordinate (RC) nor by a combination of these two quantities. For the general case with $k_1 \neq k_2$ the calculation of the transition state energy is even more complicated and can not be obtained by the calculation of energies at the known structures. Two examples of this situation are shown in Figure 4.

4. An approximation for $G^\dagger$ in the general case

Note that the expression in Eq. 3 reverts to the usual Marcus formula for $k_1 = k_2$, Eq. 2. We propose to employ an average of $\{k_1, k_2\}$ in the Marcus formula, Eq. 2, that approximates the solution for $k_1 \neq k_2$. Three different averages will be considered: an arithmetic average, a geometrical average and an arithmetic one of these two averages, as follows:

$$\begin{aligned} k^1_{avg} &= \frac{(k_1 + k_2)}{2} \\ k^2_{avg} &= \frac{(2k_1k_2)}{(k_1 + k_2)} \\ k^3_{avg} &= \frac{(k^1_{avg} + k^2_{avg})}{2} \end{aligned}$$

Figure 5 shows the relative error of the result from Marcus formula for different values of k as a function of the difference of curvatures of the two parabolas expressed as k_2/k_1. The simple arithmetic average of the two curvatures gives a very precise result when k_2/k_1 is small, until about 2. The average of the arithmetic and the geometric averages gives also very precise results for larger values of the parameter k_2/k_1. We suggest the use of these averages when Marcus formula is employed.

5. Applications for donor acceptor pairs

As mentioned above, we are interested in the application of Marcus theory to the exciton transfer between a donor molecule and an acceptor molecule in an organic photovoltaic cell. We apply the above suggested modifications of Marcus theory to two different systems. In both cases we have extended the well known "four point" method that treats the contributions of donor and acceptor to the reorganization energy separately [7], using it for the two different reorganization energies considered, i. e. those corresponding to the different parabolas.

5.1. Benzothiadiazole-thiophene and Benzopyrazine-thiophene with PCBM

Benzothiadiazole-thiophene (BTT) and Benzopyrazine-thiophene (BPT), Figure 1, are prototypical organic *small molecules* for use as donors in heterojunction organic photovoltaics (OPVs), in conjunction with PCBM as acceptor. We apply Marcus theory to the reaction

$$B?T^{*} + PCBM \rightarrow B?T + PCBM^{*}$$

for B?T either BTT or BPT. BTT and BPT have attracted attention because even though they are very similar, particularly due to the intramolecular hydrogen bond that, in principle, favours the planarity of these molecules, BTT is planar but BPT has a torsion of the rotatable bond with a dihedral angle close to 38°. This difference is not rightly predicted by some standard computational theoretical levels [8, 9]. We have calculated their structure using the highly reliable [10] ωB97X-D functional [11], obtaining the correct geometry for the ground state molecules. Singlet excited molecules for BTT and BPT, on the other hand, are both predicted to be planar. This change in geometry for the ground to excited state in BPT makes the two parabolas differ considerably thus predicting different transition state energies using one or the other parabola in traditional Marcus estimation.

Table 1 shows our results for the transition state energies predicted by employing different approximations for the curvature of the parabolic energy surfaces. As expected, predictions for BTT are very similar using the estimation based on reactants or products. Conversely, predictions for BPT differ by almost a factor of two. Our proposed combination of parabolas gives a value in between these two extremes.

5.2. Results for a representative collection of π-donors and acceptors.

We have calculated the relevant quantities for the reaction in Eq. 1 for the representative collection of π-donors and acceptors compiled by Das and Ghosh [12]. Twelve donors and twelve acceptors are presented in Figure 2. This compilation is based on the combination of well known donors based on benzene derivatives with electron-donating groups, and acceptors, similarly based on benzene derivatives, but with electron withdrawing groups. Also, other combinations are allowed in this set. For instance quinone derivatives that have been employed as acceptors in conjunction with benzene derivatives forming donors, or C_3-symmetric groups that can form stable D-A pairs. Although not all possible D-A pairs from this set have been reported, we calculate transition state energies using the Marcus approximation and the variant proposed here for all of them in order to estimate the range of the expected differences. All calculations were performed using the ωB97X-D functional.

Figure 6 shows transition state energies for all possible donor acceptor pairs from the collection with the exception of those containing acceptor A6, a dication that was not considered. In this figure we plot the prediction of the transition state energy in a candlestick style, one extreme value corresponding to the use of the reorganization energy of the reactants parabola only, the other extreme value to the use of the reorganization energy of the products and the box corresponding to the use of the averages suggested in this paper. The horizontal axis corresponds to the value of the ratio between the two reorganization energies, that is, the curvature of the two parabolas.

As expected, there is no large difference for cases where the two reorganization energies are similar ($k_2/k_1 \sim 1$), but when their ratio is appreciable different for 1, the use of an average of the two reorganization energies predicts a transition state energy vary different to either one predicted by the usual application of Marcus theory.

6. Methods

All calculations were performed using Q-Chem 4.x [13] with the ωB97X-D functional [11] and the cc-pVTZ basis set, except for when the larger PCBM molecule was included, when the 6-31G(d,p) basis set was employed.

7. Conclusions

We have presented a simple extension of the well known Marcus formula for the estimation of the rate constant of a charge transfer reaction. This approximation is in the spirit of that originally proposed by Marcus [4], for the general case in which the two parabolas involved are different, and can be applied easily to all kinds of charge transfer reactions. Results calculated for two different sets of cases of the exciton transfer in donor acceptor pairs show that this approximation modify the predicted values of the transition state energies up to a factor of two.

These results still await comparison with experiment. Also, the four point method employed for the calculation of the reorganization energy could be modified by employing the constrained density functional theory model [14].

Acknowledgments

The authors are thankful to DGTIC-UNAM for the computational resources provided and computing time under project SC16-1-IG-37. This research has been funded by CONACyT-SENER-Fondo de Sustentabilidad Energética under project 245754.

References

[1] I. V. Gopich, A. Szabo, Single-Macromolecule Fluorescence Resonance Energy Transfer and Free-Energy Profiles, The Journal of Physical Chemistry B 107 (21) (2003) 5058–5063, doi:10.1021/jp027481o.

[2] R. A. Marcus, N. Sutin, Electron transfers in chemistry and biology, BBA Reviews On Bioenergetics 811 (3) (1985) 265–322, doi: 10.1016/0304-4173(85)90014-X.

[3] P. F. Barbara, T. J. Meyer, M. A. Ratner, Contemporary Issues in Electron Transfer Research, The Journal of Physical Chemistry 100 (31) (1996) 13148–13168, doi:10.1021/jp9605663.

[4] R. A. Marcus, On the Theory of Electron-Transfer Reactions. VI. Unified Treatment for Homogeneous and Electrode Reactions, The Journal of Chemical Physics 43 (2) (1965) 679–701, doi:10.1063/1.1696792.

[5] E. Laborda, M. C. Henstridge, R. G. Compton, Asymmetric Marcus theory: Application to electrode kinetics, Journal of Electroanalytical Chemistry 667 (2012) 48–53, doi:10.1016/j.jelechem.2011.12.011.

[6] E. Laborda, M. C. Henstridge, C. Batchelor-McAuley, R. G. Compton, Asymmetric Marcus-Hush theory for voltammetry., Chemical Society reviews 42 (12) (2013) 4894–905, doi:10.1039/c3cs35487c.

[7] S. F. Nelsen, S. C. Blackstock, Y. Kim, Estimation of inner shell Marcus terms for amino nitrogen compounds by molecular orbital calculations, Journal of the American Chemical Society 109 (3) (1987) 677–682, doi: 10.1021/ja00237a007.

[8] N. E. Jackson, B. M. Savoie, K. L. Kohlstedt, M. Olvera De La Cruz, G. C. Schatz, L. X. Chen, M. a. Ratner, Controlling conformations of

conjugated polymers and small molecules: The role of nonbonding interactions, Journal of the American Chemical Society 135 (28) (2013) 10475–10483, doi:10.1021/ja403667s.

[9] J. E. Coughlin, A. Zhugayevych, R. C. Bakus, T. S. van der Poll, G. C. Welch, S. J. Teat, G. C. Bazan, S. Tretiak, A Combined Experimental and Theoretical Study of Conformational Preferences of Molecular Semiconductors, The Journal of Physical Chemistry C 118 (29) (2014) 15610–15623, doi:10.1021/jp506172a.

[10] É. Brémond, M. Savarese, N. Q. Su, Á. J. Pérez-Jiménez, X. Xu, J. C. Sancho-García, C. Adamo, Benchmarking Density Functionals on Structural Parameters of Small-/Medium-Sized Organic Molecules, Journal of Chemical Theory and Computation 12 (2) (2016) 459–465, ISSN 15499626, doi:10.1021/acs.jctc.5b01144.

[11] J.-D. Chai, M. Head-Gordon, Long-range corrected hybrid density functionals with damped atom-atom dispersion corrections, Phys. Chem. Chem. Phys. 10 (2008) 6615–6620, doi:10.1039/B810189B.

[12] A. Das, S. Ghosh, Supramolecular assemblies by charge-transfer interactions between donor and acceptor chromophores, Angewandte Chemie - International Edition 53 (8) (2014) 2038–2054, doi:10.1002/anie.201307756.

[13] Y. Shao, Z. Gan, E. Epifanovsky, A. T. Gilbert, M. Wormit, J. Kussmann, A. W. Lange, A. Behn, J. Deng, X. Feng, D. Ghosh, M. Goldey, P. R. Horn, L. D. Jacobson, I. Kaliman, R. Z. Khaliullin, T. KuÅŻ, A. Landau, J. Liu, E. I. Proynov, Y. M. Rhee, R. M. Richard, M. A. Rohrdanz, R. P. Steele, E. J. Sundstrom, H. L. W. III, P. M. Zimmerman, D. Zuev, B. Albrecht, E. Alguire, B. Austin, G. J. O. Beran, Y. A. Bernard, E. Berquist, K. Brandhorst, K. B. Bravaya, S. T. Brown, D. Casanova, C.-M. Chang, Y. Chen, S. H. Chien, K. D. Closser, D. L. Crittenden, M. Diedenhofen, R. A. D. Jr., H. Do, A. D. Dutoi, R. G. Edgar, S. Fatehi, L. Fusti-Molnar, A. Ghysels, A. Golubeva-Zadorozhnaya, J. Gomes, M. W. Hanson-Heine, P. H. Harbach, A. W. Hauser, E. G. Hohenstein, Z. C. Holden, T.-C. Jagau, H. Ji, B. Kaduk, K. Khistyaev, J. Kim, J. Kim, R. A. King, P. Klunzinger, D. Kosenkov, T. Kowalczyk, C. M. Krauter, K. U. Lao, A. D. Laurent, K. V. Lawler,

S. V. Levchenko, C. Y. Lin, F. Liu, E. Livshits, R. C. Lochan, A. Luenser, P. Manohar, S. F. Manzer, S.-P. Mao, N. Mardirossian, A. V. Marenich, S. A. Maurer, N. J. Mayhall, E. Neuscamman, C. M. Oana, R. Olivares-Amaya, D. P. OâĂŹNeill, J. A. Parkhill, T. M. Perrine, R. Peverati, A. Prociuk, D. R. Rehn, E. Rosta, N. J. Russ, S. M. Sharada, S. Sharma, D. W. Small, A. Sodt, T. Stein, D. StÃijck, Y.-C. Su, A. J. Thom, T. Tsuchimochi, V. Vanovschi, L. Vogt, O. Vydrov, T. Wang, M. A. Watson, J. Wenzel, A. White, C. F. Williams, J. Yang, S. Yeganeh, S. R. Yost, Z.-Q. You, I. Y. Zhang, X. Zhang, Y. Zhao, B. R. Brooks, G. K. Chan, D. M. Chipman, C. J. Cramer, W. A. G. III, M. S. Gordon, W. J. Hehre, A. Klamt, H. F. S. III, M. W. Schmidt, C. D. Sherrill, D. G. Truhlar, A. Warshel, X. Xu, A. Aspuru-Guzik, R. Baer, A. T. Bell, N. A. Besley, J.-D. Chai, A. Dreuw, B. D. Dunietz, T. R. Furlani, S. R. Gwaltney, C.-P. Hsu, Y. Jung, J. Kong, D. S. Lambrecht, W. Liang, C. Ochsenfeld, V. A. Rassolov, L. V. Slipchenko, J. E. Subotnik, T. V. Voorhis, J. M. Herbert, A. I. Krylov, P. M. Gill, M. Head-Gordon, Advances in molecular quantum chemistry contained in the Q-Chem 4 program package, Molecular Physics 113 (2) (2015) 184–215, doi:10.1080/00268976.2014.952696.

[14] Q. Wu, T. Van Voorhis, Direct calculation of electron transfer parameters through constrained density functional theory., J. Phys. Chem. A 110 (2006) 9212–9218, doi:10.1021/jp061848y.

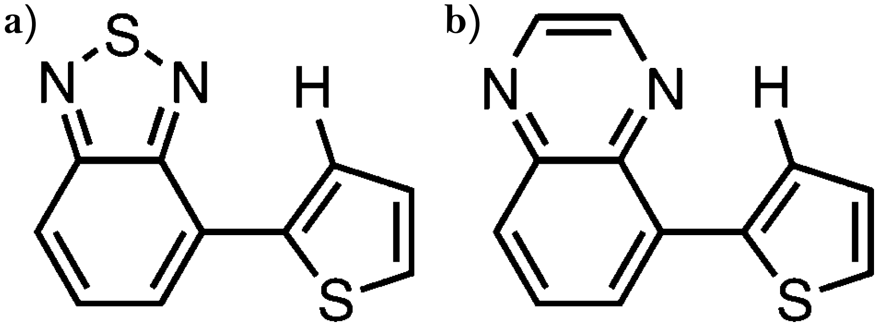

Figure 1: Structures of a) benzothiadiazole-thiophene (BTT) and b) benzopyrazine-thiophene (BPT).

approximation to λ	k	$\Delta G^\dagger$ (kcal/mol)	$\Delta G^\dagger$ (kcal/mol)
		BTT	BPT
Reactants	k_1	2.0	3.0
Products	k_2	2.9	2.9
Arithmetic mean	k^1_{avg}	2.4	3.0
Geometric mean	k^2_{avg}	2.7	2.9
Mean of means	k^3_{avg}	2.6	2.9

Table 1: Transition state energies for exciton transfer reaction for BTT + PCBM and BPT + PCBM molecules calculated by Marcus formula using different values of the approximation for the curvature of the potential energy surface.

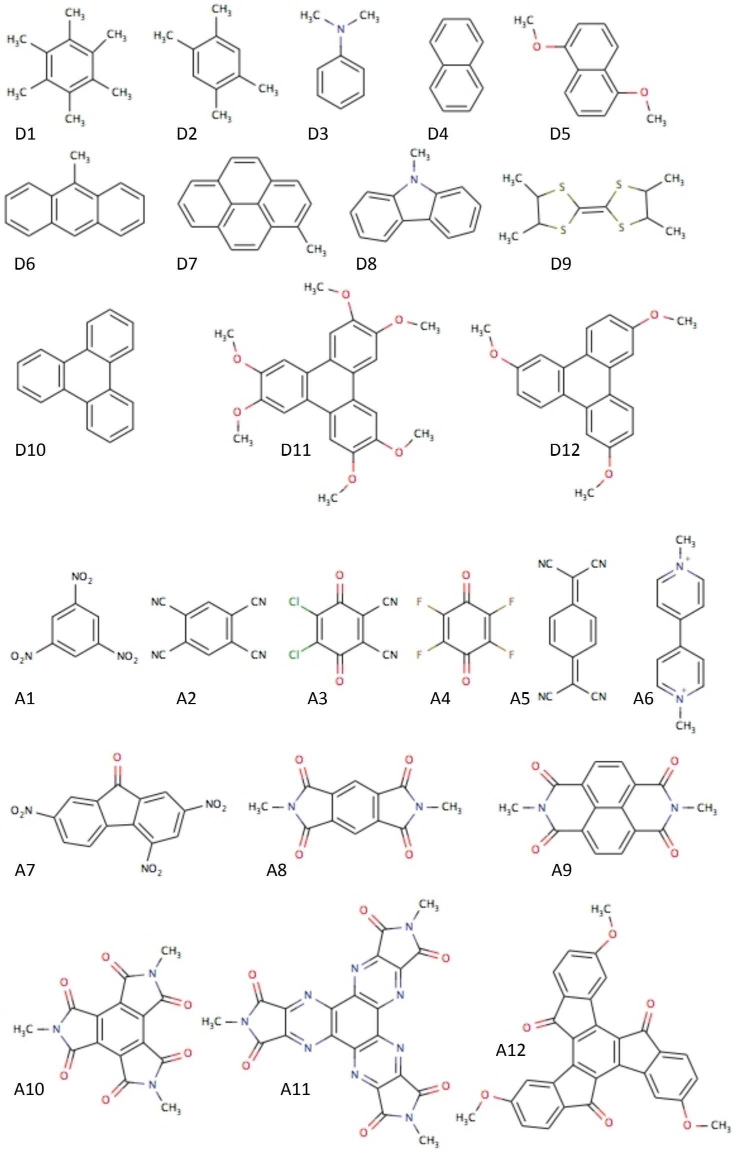

Figure 2: Structures in the set of representative π donors and acceptors calculated in this paper.

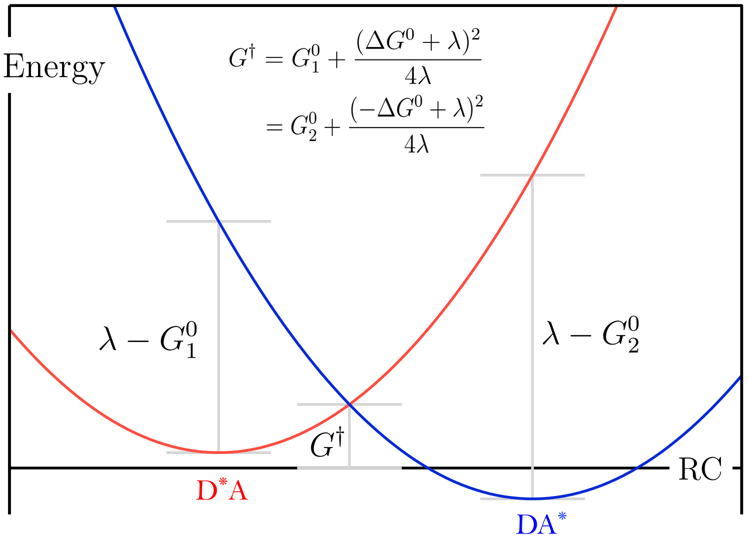

Figure 3: Parabolic potential energy surfaces for reactants and products in the reaction D*+A → D+A* as a function of reaction coordinate (RC). The curvature of the two parabolas is the same. $G^\dagger$ is given by the value of λ, available both at the reactants RC and at the products RC.

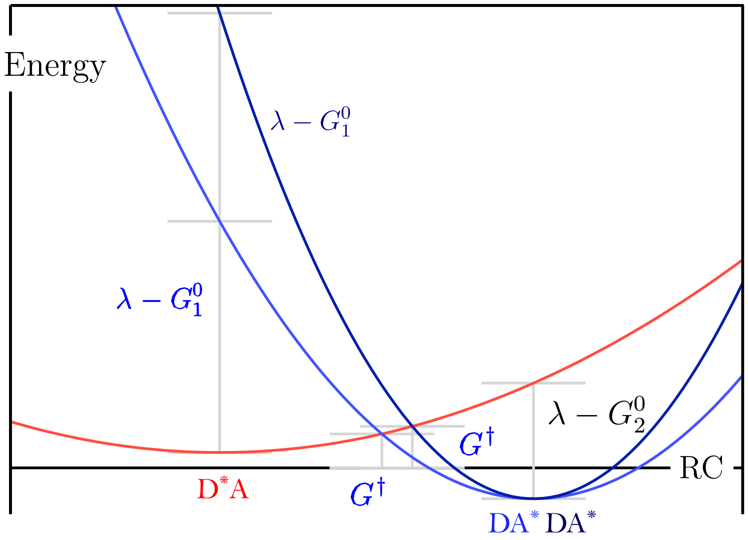

Figure 4: Parabolic potential energy surfaces for reactants and products in the reaction D*+A → D+A* as a function of reaction coordinate (RC). The curvature of the two parabolas is different and two examples are shown for the products. $G^\dagger$ is not given by the value of λ alone.

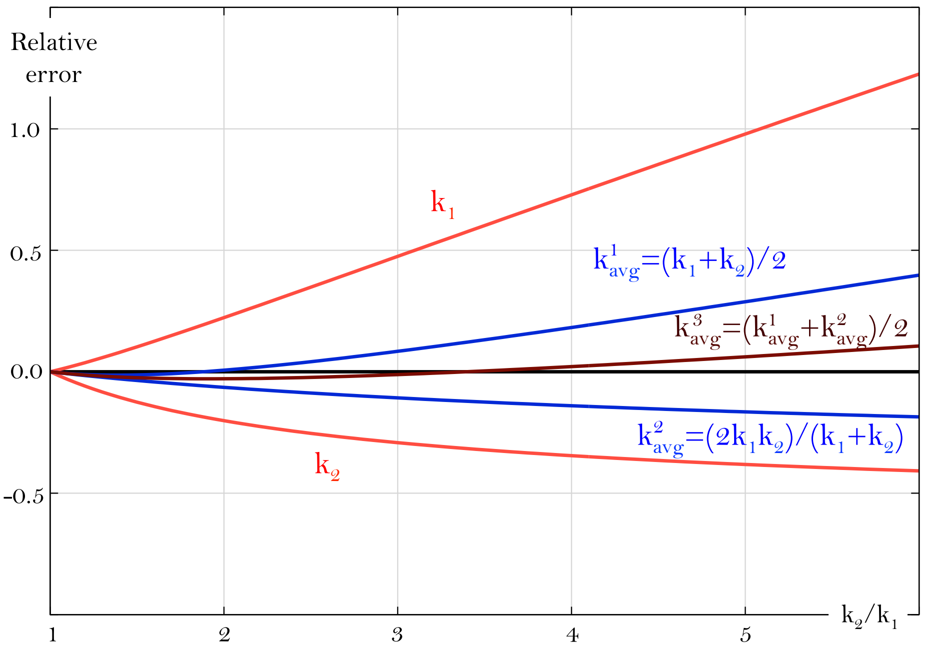

Figure 5: Relative error in the calculation of the transition state energy from Marcus formula using different averages for the curvature k. Marcus formula allows for the calculation of the transition state energy from values of energy of products and reactants at a single structure, *i. e.* at a single value of the reaction coordinate.

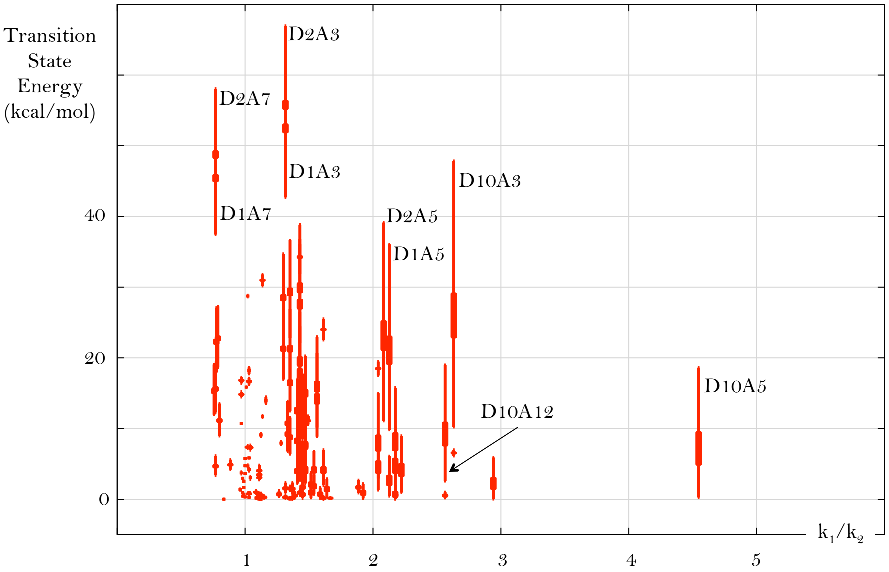

Figure 6: Transition state energies predicted by different approximations of Marcus theory for the set of donor-acceptor pairs from the collection in Fig. 2 as a function of the ratio of their reorganization energies. For some particular pairs, the use of only one reorganization energy leads to very different transition state energies, and an average should be employed.

Computational and Theoretical Chemistry 1099 (2017) 167–173

Contents lists available at ScienceDirect

Computational and Theoretical Chemistry

journal homepage: www.elsevier.com/locate/comptc

Further insights in DFT calculations of redox potential for iron complexes: The ferrocenium/ferrocene system

Martha M. Flores-Leonar, Rafael Moreno-Esparza, Víctor M. Ugalde-Saldívar *, Carlos Amador-Bedolla *

Facultad de Química, Universidad Nacional Autónoma de México, UNAM, CDMX 04510, Mexico

ARTICLE INFO

Article history:
Received 1 December 2015
Accepted 18 November 2016
Available online 19 November 2016

Keywords:
Redox potential
Ferrocenium
Ferrocene
DFT calculations

ABSTRACT

We report DFT calculations of the redox potential for the ferrocenium/ferrocene couple in acetonitrile. This system is generally used as an internal reference for non-aqueous solutions and is commonly used for redox potential determination of metal complexes. The set of functionals evaluated includes PBE, B3LYP, M05, M06, M06L and ωB97X-D along with different basis sets. Solvent effects were considered through PCM and SMD continuum models. Also, the multireference character of the system was tested. For all functionals considered structural and energetic analysis were performed in order to explain the calculated redox potentials. Results of multireference test show that a single reference treatment is adequate. A comparison between calculated and experimental parameters suggests that ωB97X-D functional in combination with SDD/cc-pVTZ basis functions and the PCM solvation model provides the best description of the redox potential and the structural and energetic parameters. Thus, a confident prediction of redox potential for the Fc^+/Fc system was obtained (0.685 V/SHE vs an experimental range of 0.624–0.650 V/SHE), which shows new insights for the widespread use of DFT calculations in the study of redox potentials for similar systems.

© 2016 Elsevier B.V. All rights reserved.

1. Introduction

Transition metal compounds have redox properties that are important for application in areas such as materials science, catalysis, environmental chemistry and so on. Some coordination compounds of the Fe(III)/Fe(II) system can exhibit those properties, so the accurate determination of their redox potential (E^0) is essential.

Experimentally the redox potential allows to describe the behavior of a chemical system in solution, related to the charge transfer throughout the electrode/electrolyte interface and is controlled by the difference in energy levels of the species in the two phases at constant T and P [1]. Currently, direct measurement of the absolute potential is not possible as it requires a reference system. Thus, what can be determined are potential differences. By convention, the H^+/H_2 is the universal reference system and the adopted electrode potential scale is based on the standard hydrogen electrode (SHE) [2], for which a zero value is established. However, experimental handling of this system is complicated and although its use is satisfactory in aqueous media it becomes unreliable in non-aqueous media. In these cases, the IUPAC recommends the use of the Fc^+/Fc redox pair (ferrocenium/ferrocene) as a reference system [3]. This system has been widely used in the determination of redox potential of different systems, particularly of coordination compounds. Although its value has been subject to some controversy, a selection of accepted values of 0.624 V/SHE [4] and 0.650 V/SHE [5] has been established.

Recently, the development of computational chemistry has allowed the description of several chemical properties among which the redox potential is of our interest. From the theoretical/-computational viewpoint, this allows to qualify the application of different approximate methods of solution to the Schrödinger equation in the description of such properties. Wave function methods offer high precision, but the computational cost is high when dealing with relatively large systems. On the other hand, a method that has been widely accepted is based on density functional theory (DFT), since it offers the best combination of accuracy and computational cost.

Several authors have calculated the value of the redox potential in acetonitrile (CH_3CN) for the Fc^+/Fc system as well as for transition metal compounds. Roy et al. [6] report potentials calculated by DFT for the Fc^+/Fc system in CH_3CN with different functionals as BLYP, BP86, PBE, B3LYP, BH&HLYP, B3P86 and PBE0. The values obtained range from −0.24 to 0.58 V/SHE, compared with the experimental value of 0.650 V/SHE [5]. According to the authors, there is no preference on the most appropriate functional for calcu-

---

* Corresponding authors.
E-mail addresses: martha14@gmail.com (M.M. Flores-Leonar), moresp@unam.mx (R. Moreno-Esparza), vmus@unam.mx (V.M. Ugalde-Saldívar), carlos.amador@unam.mx (C. Amador-Bedolla).

http://dx.doi.org/10.1016/j.comptc.2016.11.023
2210-271X/© 2016 Elsevier B.V. All rights reserved.

lating the redox potential of this system. Nevertheless, when calculating the redox potential of the metal complexes with respect to the calculated potential for Fc^+/Fc a good correlation with experimental results is obtained for the B3LYP and PBE functionals.

Namazian et al. [7], estimated the absolute redox potential for Fc^+/Fc with the use of a high level wave function method, G3 (MP2) Full-TZ-Rad, in combination with COSMO-RS as solvation model. Results are very suitable since it has a value of 0.388 V/SCE (0.632 V/SHE) against an experimental value of 0.380 V/SCE (0.624 V/SHE) [4].

According to this, it is clear that a high precision calculation may be appropriate, however it is expensive when dealing with larger systems such as various metal complexes. DFT may be suitable in calculating such systems; however, given the nature of the transition metal compounds, we wonder if their possible multireference character allows for a description based on a single-reference method such as DFT. Also, it is necessary to address in more detail the search for a more appropriate functional on the evaluation of the redox potential for the Fc^+/Fc system to properly describe this property on metal complexes.

We are interested in correctly describe redox properties of various Fe(III)/Fe(II) coordination compounds [8], for which, it was observed that the relationship between structure and redox potential seems to be significant. For that purpose we require a functional able to correctly describe these properties.

Therefore, the general purpose of our study is to evaluate different DFT approaches in calculating redox potential as well as both structural and energetic parameters of the Fc^+/Fc system to find out those with the best performance. Once an adequate methodology is found, we intend to use it in further work that allows us to predict the effects of chemical variations (for example: ligand substitutions, ligand aliphatic chain length variation, the use of chelating ligands, etc.) on the calculation of redox potentials of iron complexes, with good structural predictions and relatively low computational cost.

It is worth mentioning that the structural arrangement of the Fc^+/Fc system and of most of the transition metal complexes we want to apply this methodology to, depends on non covalent interactions amongst the coordinated ligands. So a functional which includes dispersion corrections may be needed, not only for the appropriate description of the structural arrangements but, through this, of other properties of interest (e.g. magnetic properties) also observed in the iron complexes.

1.1. The redox potential

As mentioned above, experimentally it is not possible to determine an absolute potential, it is necessary to employ a reference. In this way, the redox potential (E_{redox}) is the difference of the potential between two half-reactions, the system of interest (E_{abs}) and a reference system (E_{ref}), as shown in Eqs. (1)–(3),

$$\mathrm{Ox} + e^- \longrightarrow \mathrm{Red}^- \quad E_{abs} \tag{1}$$

$$\mathrm{Ox}_{ref} + e^- \longrightarrow \mathrm{Red}^-_{ref} \quad E_{ref} \tag{2}$$

$$\mathrm{Ox} + \mathrm{Red}^-_{ref} \longrightarrow \mathrm{Red}^- + \mathrm{Ox}_{ref} \quad E_{redox} = E_{abs} - E_{ref}. \tag{3}$$

One method for determining the redox potential of a system is to calculate the potential of the two half-reactions and subtract them to get the redox potential of the system. This method, known as isodesmic [9], has the advantage that it is possible to minimize systematic errors as the difference between E_{ref} and E_{abs} leads to error cancellations. It is worth mentioning that this method is most commonly used when trying to determine the redox potential in non-aqueous media of transition metals compounds with Fc^+/Fc reference system as it is done experimentally. An adequate calculation of the redox potential for the Fc^+/Fc system is of importance for determining the redox potential of different metal complexes.

1.2. The Born-Haber cycle

For the calculation of redox potentials, a Born-Haber cycle has been proposed and employed by several authors [6,7,9]. This thermodynamical cycle is shown in Fig. 1; there, the quantity of interest is the standard Gibbs free energy of redox half reaction in solution $\Delta G^{o,\ redox}_{solv}$. According to the cycle, this is obtained by calculating the change in free energy in gas phase $\Delta G^{o,\ redox}_{gas}$ and the solvation free energies of each of the species ΔG^{o}_{solv} (Red) and ΔG^{o}_{solv} (Ox). The overall balance is shown in Eq. (4),

$$\Delta G^{o,\ redox}_{solv} = \Delta G^{o,\ redox}_{gas} + \Delta G^{o}_{solv}(Red) - \Delta G^{o}_{solv}(Ox) \tag{4}$$

Finally, to calculate the redox potential of a half reaction for a single electron, Eq. (5) known as the Nernst equation is used, where F is the Faraday constant,

$$\Delta G^{o,\ redox}_{solv} = -FE^{o}_{calc}. \tag{5}$$

2. Computational methods

DFT calculations were performed with Gaussian 09 (version C.01) package [10] with the following specifications.

2.1. Functionals and basis sets

Six different functionals were examined. The GGA functional PBE [11]. The hybrid functional B3LYP [12]. From the Minnesota series, the hybrid functionals M05, M06 and the pure functional M06L [13–15]. Finally the long range corrected functional with dispersion corrections ωB97X-D [16]. Three basis sets of increasing size were considered. Two of them including an effective core potential for the iron atom and all electron for cyclopentadienyl (Cp) rings: LANL08 [17]/6-311G* [18] and SDD [19]/cc-pVTZ [20] for Fe/Cp. The third basis set was an all electron Def2-TZVP [21] which was employed only for the B3LYP and ωB97X-D since these were the best functionals observed.

2.2. Geometries and free energies

Geometries of ferrocene (Cp_2Fe) and ferrocenium ($[Cp_2Fe]^+$) in the eclipsed conformation (D_{5h}) were optimized in gas phase.

Solvent effects were included using the PCM and SMD methods [22,23] as implemented in Gaussian 09. In solution two geometries were calculated, the single point gas phase geometries (SP) and full optimized geometries (OPT), using acetonitrile (CH_3CN) as solvent.

The gas phase and solvation free energies of each species were evaluated through a thermochemical analysis at 298.15 K and 1 atm of the aforementioned geometries in order to obtain the free energy differences of the cycle, $\Delta G^{o,\ redox}_{gas}$, ΔG^{o}_{solv} (Red) and ΔG^{o}_{solv} (Ox).

$$\begin{tikzcd}
\mathrm{Ox}_g + e^-_g \arrow[r, "\Delta G^{o,\ redox}_{gas}"] \arrow[d, "\Delta G^{o}_{solv}(\mathrm{Ox})"'] & \mathrm{Red}_g \arrow[d, "\Delta G^{o}_{solv}(\mathrm{Red})"] \\
\mathrm{Ox}_{solv} + e^-_g \arrow[r, "\Delta G^{o,\ redox}_{solv}"'] & \mathrm{Red}_{solv}
\end{tikzcd}$$

Fig. 1. The Born-Haber cycle.

2.3. Multireference calculations

In addition, the multireferential character of the system Fc^+/Fc was evaluated with the A_λ diagnostic proposed by Fogueri et al. [24].

3. Results and discussion

3.1. Multireference character

As mentioned previously, DFT properly describes several chemical systems at low computational cost. However, such systems correspond to those in which dynamic correlation effects predominate. This is due to the single-reference nature of its formulation.

Systems with transition metals, particularly *3d* metals, may exhibit significant nondynamical electron correlation effects that single-referential methods do not describe well. To treat such systems a multi-referential calculation is required. However, it is known that for large systems the computational cost can be expensive.

To evaluate the multireferential character of a system, many diagnostics have been proposed. Most of them based on multiconfiguration self-consistent field calculations. However, other diagnostics use DFT calculations, with the advantage of lower computational cost.

In this paper the A_λ diagnostic was evaluated. This was proposed by Fogueri et al. [24] and is a measure of the nondynamical correlation effects, which are estimated through Eq. (6),

$$A_\lambda = \left(1 - \frac{TAE[X_\lambda C]}{TAE[XC]}\right)\frac{1}{\lambda}, \tag{6}$$

where TAE is the molecular total atomization energy, XC is a pure DFT exchange correlation functional and $X_\lambda C$ is the corresponding hybrid with 100λ % Hartree Fock exchange. In this diagnostic, values of A_λ from 0 to 0.1 indicate that correlation is predominantly dynamic and thus of non-multireference character. Results are shown in Table 1 for three basic functionals and for the two systems involved in this paper.

The A_λ diagnostic, being a relative amount makes it an appropriate way of determining the multireferential character. Results show values within the expected range for a dynamic correlation in the case of ferrocene. For ferrocenium, the value for the PBE0/PBE couple lies in the limit for a dynamic correlation, however, for other functionals, values are within the expected range. Thus, a DFT single-reference calculation can be used in the treatment of such systems.

3.2. Geometries

Ferrocene is an organometallic compound comprising an iron II (Fe^{2+}) metal ion bonded to two cyclopentadienyl rings (Cp^-) through η^5 bonds in a "sandwich" structure. This compound may have different conformations, going from one in which the two Cp rings are eclipsed (D_{5h}) to another in a staggered arrangement (D_{5d}). In solid state it is possible to observe these conformations in any of the three phases in which ferrocene can crystalize [25]. Among these, below 242 K, the orthorhombic phase has molecules in the eclipsed conformation. Furthermore, in gas phase, the most stable conformation of ferrocene corresponds to the eclipsed (D_{5h}), as determined by Bohn and Haaland in a gas-phase electron diffraction (GED) study [26], this was later confirmed by Coriani et al. [27] by calculations at MP2, CCSD and CCSD(T) levels of theory.

According to the above, the D_{5h} conformation was considered in this study for ferrocene and ferrocenium structures. These structures were optimized in gas phase (starting from an X-ray structure), for all different functionals with the LANL08/6-311G* and SDD/cc-pVTZ basis sets; and for B3LYP and ωB97X-D with Def2-TZVP basis. For comparison purposes three typical bond distances corresponding to the Fe—Cp, Fe—C and C—C distances were selected. Complete average distances for the ferrocene structure are available in supporting information (Table SI 1). The results are compared with CCSD(T) calculations performed by Coriani et al. [27] and experimental values obtained from a weighted average of different X-ray structures [28,29] (Table SI 3).

To observe the performance of the functionals, an analysis of the mean unsigned error percentage (% MUE) were done, showing the best functionals for the three bond distances. In Fig. 2 the % MUE for the six functionals are plotted for the ferrocene structure with different color each. The standard deviation expressed as a percentage (% σ) obtained from the weighted average of the experimental values is plotted in black as well as the %MUE of the CCSD (T) calculations in gray.

For the basis sets an improvement when going from LANL08/6-311G* to SDD/cc-pVTZ was observed for the PBE, M05, M06 and M06L functionals. However, the basis set size seems not to have a significant effect for B3LYP and ωB97X-D. In these cases, a recalculation with Def2-TZVP basis was made which slightly reduces the %MUE in the three bond distances reported. Most remarkable in the graph is that some of the functionals are found near the experimental deviation range, in particular the ωB97X-D have errors even lower that the CCSD(T) method with the LANL08/6-311G* basis for the three distances. The PBE and the M06 functionals also have a good performance. On the other hand, B3LYP functional has the largest errors for the Fe—Cp and the Fe—C distances with a SDD/cc-pVTZ basis.

For the ferrocenium ion structure, geometries were also optimized and in order to compare with experimental values, as reported for ferrocene above, a weighted average of X-ray structures was obtained (see Table SI 4). The comparison with experiment is a little more involved as crystals of ferrocenium have been prepared with different counterions. A group with hexabromo- and hexachloro-rhenium (IV) as counterion was chosen because these were the most ionic anions [30]. Comparing to ferrocene, the experimental average distance Fe—Cp slightly increases from 1.650 to 1.692 Å, in the same way the Fe—C distance increases from 2.045 to 2.079 Å, while the C—C distance shows a

Table 1
A_λ diagnostic for ferrocene and ferrocenium with B3LYP/BLYP, M06/M06L and PBE0/PBE functionals.

Functional	100λ %	Ferrocene		Ferrocenium	
		TAE (kJ/mol)	A_λ	TAE (kJ/mol)	A_λ
B3LYP	20	−9678.017	−0.011	−8994.252	0.024
BLYP	0	−9655.967		−9037.977	
M06	28	−9695.346	0.075	−9067.389	0.081
M06L	0	−9902.648		−9277.980	
PBE0	25	−9927.560	0.096	−9253.300	0.117
PBE	0	−10171.948		−9532.491	

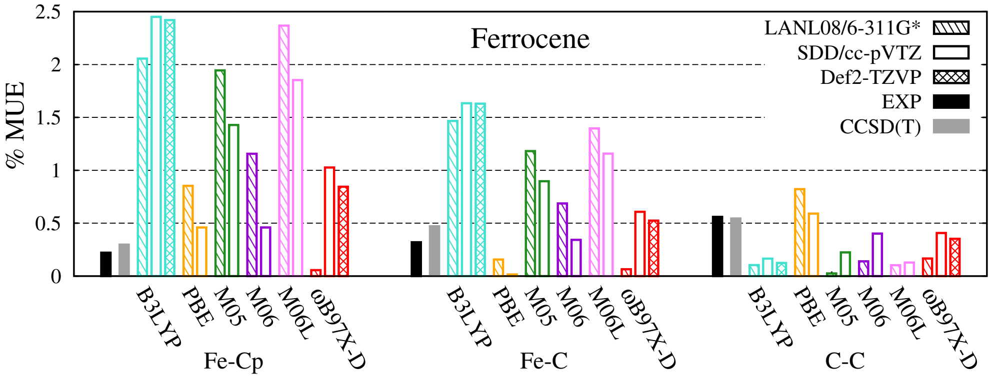

Fig. 2. Bond length mean unsigned error percentage (%MUE) for all functionals for ferrocene with LANL08/6-311G, SDD/cc-pVTZ and Def2-TZVP basis sets. Comparison with CCSD(T) calculations and the average of the experimental values, the bar corresponds to their percentage of standard deviation (% σ).

reduction from 1.425 to 1.420 Å (complete distances for ferrocenium are reported in Table SI 2).

It was also observed that the percentage of standard deviation (% σ) of the experimental data in the case of ferrocenium is greater than for ferrocene, as can be seen in Fig. 3. In these cases, the % MUE are comparable to the experimental % σ. Improving the basis set to a SDD/cc-pVTZ is possible to appreciate a decrease in the mean errors. In this case, M06 and M06L functionals have the lowest values. Additionally, note that the ωB97X-D functional also has a good performance with a mean error lower than the experimental deviation for the three distances.

3.3. Free energies differences (ΔG)

Before obtaining the redox potential of Fc$^+$/Fc system, it is convenient to analyze the free energies differences involved in the Born-Haber cycle. Free energies were obtained through a thermochemical analysis as implemented in Gaussian 09. The electronic, rotational and vibrational corrections, which include the zero point energy correction, were calculated at 298.15 K. The gas phase free energy difference, $\Delta G^{o,\,redox}_{gas}$, was obtained from the optimized geometry of both ferrocene and ferrocenium ion. The ΔG^{o}_{solv} (Ox) and ΔG^{o}_{solv} (Red) were obtained in two ways, from a single point calculation using the optimized gas phase geometry (SP) and by a full geometry optimization in solution (OPT) with the PCM and SMD solvation models. The solvent employed was acetonitrile (CH_3CN, $\varepsilon = 35.688$). From these three quantities $\Delta G^{o,\,redox}_{solv}$ was obtained through Eq. (4).

We observed that using the SDD/cc-pVTZ basis set and PCM as solvation model the best results are obtained (see extended tables of energies in SI 5 and SI 6). Results are summarized in Table 2 for the six functionals. One can observe that the gas phase free energy differences, $\Delta G^{o,\,redox}_{gas}$, calculated with different functionals, have the largest variations. These values are compared with experimental ionization energies; the reported values vary from 636.813 to 694.706 kJ/mol (6.6 to 7.2 eV) [31], from these, the negative value was taken for comparative purposes. In this case, the functionals that are within the range of the experimental value are B3LYP and ωB97X-D with −681.834 and −685.633 kJ/mol respectively, all other functionals are above the range reported.

For the solvation free energies ΔG^{o}_{solv} (Ox) and ΔG^{o}_{solv} (Red) corresponding to ΔG^{o}_{solv} (Fc$^+$) and ΔG^{o}_{solv} (Fc) respectively, the observed variation on the calculated values is less than in the gas phase. Furthermore, there is an improvement when performing a geometry optimization in solution instead of a single point calculation (see Table SI 5). For ferrocenium no experimental solvation free energies were found, ΔG^{o}_{solv} (Fc$^+$), these were estimated through the Born-Haber cycle using the available experimental values: $\Delta G^{o,\,redox}_{gas}$ from −636.813 to −694.706 kJ/mol [31], ΔG^{o}_{solv} (Fc) = −32.029 kJ/mol [32] and $\Delta G^{o,\,redox}_{solv} = -506.548$ kJ/mol, obtained from the experimental redox potential of 0.650 V/SHE [5]. We observed that calculations with PCM model are in agreement with the estimated range from −162.283 to −220.176 kJ/mol except for M06L functional which markedly overestimates this value.

For ferrocene the solvation free energy, ΔG^{o}_{solv} (Fc), is overestimated in all cases with this combination of basis set

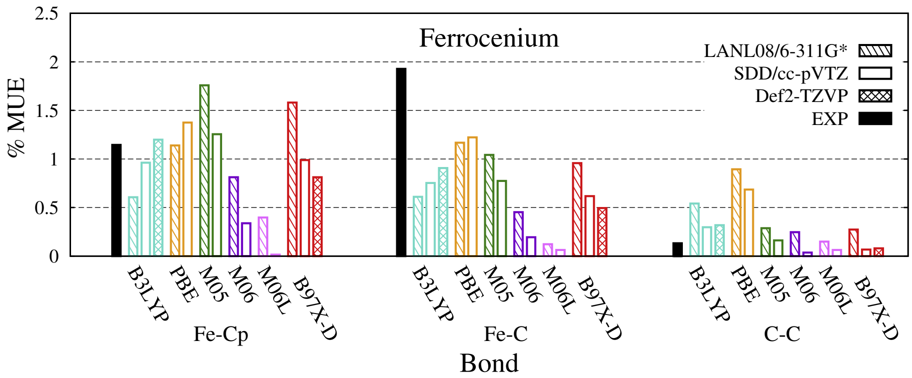

Fig. 3. Bond length mean unsigned error percentage (%MUE) for all functionals for ferrocenium with LANL08/6-311G, SDD/cc-pVTZ and Def2-TZVP basis sets. Comparison with the average of the experimental values, the bar corresponds to their percentage of standard deviation (% σ).

Table 2
Calculated and experimental free energies in gas phase ($\Delta G^{o,\,redox}_{gas}$) and in CH_3CN (ΔG^{o}_{solv} and $\Delta G^{o,\,redox}_{solv}$) for Fc^+/Fc pair (kJ/mol).

Functional	SDD/cc-pVTZ			
	GP-OPT	PCM-OPT		
	$\Delta G^{o,\,redox}_{gas}$	ΔG^{o}_{solv} (Fc^+)	ΔG^{o}_{solv} (Fc)	$\Delta G^{o,\,redox}_{solv}$
B3LYP	−681.834	−185.854	−11.090	−507.071
PBE	−634.793	−175.310	−11.704	−471.188
M05	−613.637	−178.786	−10.473	−445.324
M06	−622.755	−182.417	−10.376	−450.714
M06L	−623.168	−140.483	−8.493	−491.178
ωB97X-D	−685.633	−187.343	−11.644	−509.935
EXP	−636.813[a]	−162.283[b]	−32.029[c]	−504.039[d]
	−694.706[a]	−220.176[b]		−506.548[e]

[a] The negative value of ionization energy range reported [31].
[b] Calculated using the Born-Haber cycle with $\Delta G^{o,\,redox}_{gas}$ obtained from [31], ΔG^{o}_{solv} (Fc) obtained from [32] and $\Delta G^{o,\,redox}_{solv}$ from [5].
[c] Ref. [32].
[d] Calculated from the experimental redox potential value of 0.624 V/SHE [4].
[e] Calculated from the experimental redox potential 0.650 V/SHE [5].

(SDD/cc-pVTZ) and PCM solvation model. It was found a similar behavior for the LANL08/6-311G* and Def2-TZVP basis sets. If solvation model is changed to SMD, energies nearest to the experimental value were found, despite this improvement, values of Gibbs free energies of redox half reaction, $\Delta G^{o,\,redox}_{solv}$, are further away from the experimental (Table SI 6).

Finally, from the overall balance, the standard Gibbs free energy of redox half reaction in solution, $\Delta G^{o,\,redox}_{solv}$, is determined. Differences between the gas phase optimized values and the complete optimized ones in solution were found, in almost all cases a value closer to the experimental is obtained by performing a complete optimization (see Table SI 5). Once again the B3LYP and ωB97X-D are the most approximate to the experimental values. We believe that a major source of error lies in the calculation of the gas phase free energy, as it is the one with the largest variations.

3.4. Redox potentials (E^0)

Using the free energies of redox half reaction in solution $\Delta G^{o,\,redox}_{solv}$, the redox potential ($E^0$) is determined through Eq. (5) and the values obtained are referenced to the standard hydrogen electrode (SHE) in acetonitrile, whose absolute value is 4.6 V [1]. As previously mentioned, several different redox potentials are reported in the literature, we compare with some of the most recent and recommended values being 0.624 V/SHE [4] and 0.650 V/SHE [5].

Comparing the potentials obtained from a GP-OPT and a the potentials obtained from a complete optimization (GP-OPT & PCM-OPT), the values closer to the experimental are obtained from the latter (see Tables SI 7 and SI 8). In Table 3 results are presented for the six functionals, the basis sets and a full optimized structure in both gas phase and acetonitrile with PCM as solvation model.

It is possible to observe that increasing the basis from LANL08/Cp:6-311G* to SDD/cc-pVTZ the redox potential presents an improvement and values of 0.655 V/SHE and 0.685 V/SHE are obtained for B3LYP and ωB97X-D, however when the Def2-TZVP is used this value is overestimated in both cases. It is clear that the choice of the functional plays the most important role on the calculation of redox potentials. To better observe the performance of all functionals, values were plotted in a redox potential scale (Fig. 4), using the three basis sets and PCM as solvation model. The experimental values are shown in solid black lines.

Table 3
Calculated values of E^0 (V/SHE) for Fc^+/Fc in acetonitrile (CH_3CN).[a] Comparison between experimental (EXP), in italics, and calculated values for all functionals and basis sets (values closer to experimental are in bold) with PCM as solvation model.

Functional	GP-OPT & PCM-OPT		
	Fe:LANL08/Cp:6-311G*	Fe:SDD/Cp:cc-pVTZ	Def2-TZVP
B3LYP	**0.751**	**0.655**	**0.714**
PBE	0.305	0.284	–
M05	0.122	0.015	–
M06	0.264	0.071	–
M06L	0.653	0.491	–
ωB97X-D	**0.919**	**0.685**	**0.741**
EXP	***0.624*** [4] and ***0.650*** [5]		

[a] SHE in CH_3CN is 4.6 V [1].

From the graph, what is most striking is the proximity of B3LYP with SDD/cc-pVTZ basis (0.655 V/SHE) to the experimental values. This is not surprising since it has been one of the most successful and perhaps the most popular functional since its introduction in 1993 by Becke [12]. However, as A. J. Cohen et al. mentioned [33], one of the challenges of DFT is to develop a functional that performs better than B3LYP. In the graph, the M06L functional in combination with LANL08/6-311G* also is very near to the experimental, however its performance with geometries and energies is not remarkable. On the other hand, ωB97X-D with SDD/cc-pVTZ basis also has an excellent performance in predicting the redox potential with a value of 0.685 V/SHE. Moreover, this functional has proved to be the most consistent throughout the analysis of geometries, energies and redox potentials made in this paper. This achievement could be attributed to the nature of the functional, as it is located on a higher rung of the DFT Jacob's ladder proposed by Perdew and Schmidt [34].

Lastly, it is noteworthy that the difference between the two of the best values obtained from calculations (B3LYP and ωB97X-D with SDD/cc-pVTZ basis), is 0.030 V/SHE. It is of the same order as the difference between two reliable experimental values, 0.026 V/SHE. Thus, this study shows that DFT approaches can adequately estimate values of redox potential, particularly the Fc^+/Fc couple, which is used as a reference system to calculate redox potentials of coordination compounds. Also, with the approximations established here, the importance of this work is to apply this methodology to calculate and predict accurate redox potentials on several iron coordination compounds as the studied in Ref. [8], and if it is possible explain other properties observed such as magnetics.

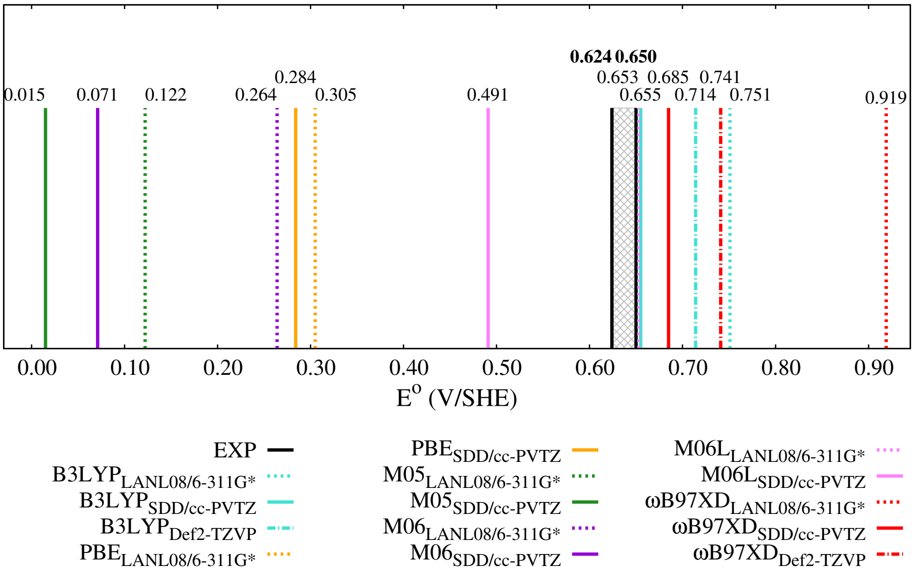

Fig. 4. Redox potential scale for Fc^+/Fc calculated vs experimental for all functionals with SDD/cc-pVTZ basis set and PCM solvation model.

4. Conclusions

It was shown that it is possible to perform adequate calculations of the redox potential for the Fc^+/Fc system within the framework of a single-reference method such as density functional theory (DFT).

Methodological analyses of structure, energy and redox potential were performed for different DFT approaches. It is observed that some functionals correctly describe structural or energetic parameters, however fail in the description of redox potential, between them, we recommend the use of ωB97X-D, since it has proved to be consistent throughout the analysis and in combination with a basis set SDD and cc-pVTZ for Fe and Cp respectively and PCM solvation model, a good redox potential value is obtained for the Fc^+/Fc system (0.685 V/SHE). The inclusion of a dispersion term in ωB97X-D allowed for the calculation of its geometry in very close agreement with experimental values. Also, the fact that the difference between the best calculated values and reliable experimental values are comparable, support the calculation of redox potentials through DFT approaches.

Thereby, this work presents a new scenario into the DFT calculations of redox potential, showing that it is possible to obtain a reliable value for the Fc^+/Fc system in acetonitrile, which can be used as a reference for the calculation of redox potential of coordination compounds, particularly in order to estimate the effect of chemical variations such as ligand substitutions, ligand aliphatic chain length variation and chelating ligands which will be better described by a density functional that includes non covalent interactions.

Conflict of interest

The authors declare no competing financial interest.

Acknowledgements

We acknowledge supercomputer services provided by DGTIC-UNAM (Miztli 1538-2015). M.M.F.-L. thanks CONACYT for financial support under scholarship number 240090.

Appendix A. Supplementary material

Supplementary data associated with this article can be found, in the online version, at http://dx.doi.org/10.1016/j.comptc.2016.11.023.

References

[1] S. Trasatti, The absolute electrode potential: an explanatory note (Recommendations 1986), Pure Appl. Chem. 58 (7) (1986) 955–966.

[2] R.W. Ramette, Outmoded terminology: the normal hydrogen electrode, J. Chem. Educ. 64 (10) (1987) 885.

[3] G. Gritzner, J. Kûta, Recommendations on reporting electrode-potentials in nonaqueous solvents (Recommendations 1983), Pure Appl. Chem. 56 (4) (1984) 461–466.

[4] V.V. Pavlishchuk, A.W. Addison, Conversion constants for redox potentials measured versus different reference electrodes in acetonitrile solutions at 25 °C, Inorg. Chim. Acta 298 (2000) 97–102.

[5] N.G. Connelly, W.E. Geiger, Chemical redox agents for organometallic chemistry, Chem. Rev. 96 (2) (1996) 877–910.

[6] L.E. Roy, E. Jakubikova, M.G. Guthrie, E.R. Batista, Calculation of one-electron redox potentials revisited. Is it possible to calculate accurate potentials with density functional methods?, J Phys. Chem. A 113 (24) (2009) 6745–6750.

[7] M. Namazian, C.Y. Lin, M.L. Coote, Benchmark calculations of absolute reduction potential of ferricinium/ferrocene couple in nonaqueous solutions, J. Chem. Theory Comput. 6 (9) (2010) 2721–2725.

[8] N. Ortega-Villar, A.Y. Guerrero-Estrada, L. Piñeiro-López, M.C. Muñoz, M. Flores-Álamo, R. Moreno-Esparza, J.A. Real, V.M. Ugalde-Saldívar, Spin crossover behavior in a series of iron(III) alkoxide complexes, Inorg. Chem. 54 (7) (2015) 3413–3421.

[9] K. Arumugam, U. Becker, Computational redox potential predictions: applications to inorganic and organic aqueous complexes, and complexes adsorbed to mineral surfaces, Minerals 4 (2) (2014) 345–387.

[10] M.J. Frisch, G.W. Trucks, H.B. Schlegel, G.E. Scuseria, M.A. Robb, J.R. Cheeseman, G. Scalmani, V. Barone, B. Mennucci, G.A. Petersson, H. Nakatsuji, M. Caricato, X. Li, H.P. Hratchian, A.F. Izmaylov, J. Bloino, G. Zheng, J.L. Sonnenberg, M. Hada, M. Ehara, K. Toyota, R. Fukuda, J. Hasegawa, M. Ishida, T. Nakajima, Y. Honda, O. Kitao, H. Nakai, T. Vreven, J.J.A. Montgomery, J.E. Peralta, F. Ogliaro, M. Bearpark, J.J. Heyd, E. Brothers, K.N. Kudin, V.N. Staroverov, T. Keith, R. Kobayashi, J. Normand, K. Raghavachari, A. Rendell, J.C. Burant, S.S. Iyengar, J. Tomasi, M. Cossi, N. Rega, J.M. Millam, M. Klene, J.E. Knox, J.B. Cross, V. Bakken, C. Adamo, J. Jaramillo, R. Gomperts, R.E. Stratmann, O. Yazyev, A.J. Austin, R. Cammi, C. Pomelli, J.W. Ochterski, R.L. Martin, K. Morokuma, V.G. Zakrzewski, G.A. Voth, P. Salvador, J.J. Dannenberg, S. Dapprich, A.D. Daniels, O. Farkas, J.B. Foresman, J.V. Ortiz, J. Cioslowski, D.J. Fox, Gaussian 09 Revision C.01, Gaussian Inc. Wallingford CT, 2010.

[11] J. Perdew, K. Burke, M. Ernzerhof, Generalized gradient approximation made simple, Phys. Rev. Lett. 77 (18) (1996) 3865–3868.

[12] A.D. Becke, Density-functional thermochemistry. III. The role of exact exchange, J. Chem. Phys. 98 (7) (1993) 5648.

[13] Y. Zhao, N.E. Schultz, D.G. Truhlar, Exchange-correlation functional with broad accuracy for metallic and nonmetallic compounds, kinetics, and noncovalent interactions, J. Chem. Phys. 123 (16) (2005) 161103.
[14] Y. Zhao, D.G. Truhlar, The M06 suite of density functionals for main group thermochemistry, thermochemical kinetics, noncovalent interactions, excited states, and transition elements: two new functionals and systematic testing of four M06-class functionals and 12 other functionals, Theor. Chem. Acc. 120 (1) (2008) 215–241.
[15] Y. Zhao, N.E. Schultz, D.G. Truhlar, Design of density functionals by combining the method of constraint satisfaction with parametrization for thermochemistry, thermochemical kinetics, and noncovalent interactions, J. Chem. Theory Comput. 2 (2) (2006) 364–382.
[16] J.-D. Chai, M. Head-Gordon, Systematic optimization of long-range corrected hybrid density functionals, J. Chem. Phys. 128 (8) (2008) 084106.
[17] L.E. Roy, P.J. Hay, R.L. Martin, Revised basis sets for the LANL effective core potentials, J. Chem. Theory Comput. 4 (7) (2008) 1029–1031.
[18] R. Krishnan, J.S. Binkley, R. Seeger, J.A. Pople, Self-consistent molecular orbital methods. XX. A basis set for correlated wave functions, J. Chem. Phys. 72 (1) (1980) 650.
[19] M. Dolg, U. Wedig, H. Stoll, H. Preuss, Energy-adjusted ab initio pseudopotentials for the first row transition elements, J. Chem. Phys. 86 (2) (1987) 866.
[20] T.H. Dunning, Gaussian basis sets for use in correlated molecular calculations. I. The atoms boron through neon and hydrogen, J. Chem. Phys. 90 (2) (1989) 1007.
[21] F. Weigend, R. Ahlrichs, Balanced basis sets of split valence, triple zeta valence and quadruple zeta valence quality for H to Rn: design and assessment of accuracy, Phys. Chem. Chem. Phys. 7 (18) (2005) 3297–3305.
[22] J. Tomasi, B. Mennucci, R. Cammi, Quantum mechanical continuum solvation models, Chem. Rev. 105 (8) (2005) 2999–3093.
[23] A.V. Marenich, C.J. Cramer, D.G. Truhlar, Universal solvation model based on solute electron density and on a continuum model of the solvent defined by the bulk dielectric constant and atomic surface tensions, J. Phys. Chem. B 113 (18) (2009) 6378–6396.
[24] U.R. Fogueri, S. Kozuch, A. Karton, J.M.L. Martin, A simple DFT-based diagnostic for nondynamical correlation, Theor. Chem. Acc. 132 (1) (2012) 1291.
[25] M. Appel, B. Frick, T.L. Spehr, B. Stühn, Molecular ring rotation in solid ferrocene revisited, J. Chem. Phys. 142 (11) (2015) 114503.
[26] R.K. Bohn, A. Haaland, On the molecular structure of ferrocene, $Fe(C_5H_5)_2$, J. Organomet. Chem. 5 (5) (1966) 470–476.
[27] S. Coriani, A. Haaland, T. Helgaker, P. Jørgensen, The equilibrium structure of ferrocene, ChemPhysChem 7 (1) (2006) 245–249.
[28] P. Seiler, J.D. Dunitz, The structure of triclinic ferrocene at 101, 123 and 148 K, Acta Crystallogr., Sect. B: Struct. Crystallogr. Cryst. Chem. 35 (9) (1979) 2020–2032.
[29] P. Seiler, J.D. Dunitz, Low-temperature crystallization of orthorhombic ferrocene: structure analysis at 98 K, Acta Crystallogr., Sect. B: Struct. Crystallogr. Cryst. Chem. 38 (6) (1982) 1741–1745.
[30] R. González, R. Chiozzone, C. Kremer, F. Guerra, G. De Munno, F. Lloret, M. Julve, J. Faus, Magnetic studies on hexahalorhenate(IV) salts of ferrocenium cations $[Fe(C_5R_5)_2]_2[ReX_6]$ (R = H, CH_3; X = Cl, Br, I), Inorg. Chem. 43 (9) (2004) 3013–3019.
[31] J.A. Martinho Simões, NIST Chemistry WebBook, NIST Standard Reference Database Number 69, Gaithersburg, MD, 20899 (Chapter Organometallic Thermochemistry Data). <http://webbook.nist.gov>.
[32] A.M. Kuznetsov, A.N. Maslii, L.I. Krishtalik, Quantum chemical model of solvation for calculation of electrode potentials of redox processes involving ferrocene, cobaltocene, and their ions, Russ. J. Electrochem. 44 (2008) 34–42.
[33] A.J. Cohen, P. Mori-Sánchez, W. Yang, Challenges for density functional theory, Chem. Rev. 112 (1) (2012) 289–320.
[34] J.P. Perdew, K. Schmidt, Density Functional Theory and Its Applications to Materials, American Institute of Physics, Melville, NY, 2001.

Correlating properties in iron(III) complexes: A DFT description of structure, redox potential and spin crossover phenomena

Martha M. Flores-Leonar[a], Rafael Moreno-Esparza[a], Víctor M. Ugalde-Saldívar*[a], and Carlos Amador-Bedolla*[a]

Abstract: Calculations of structure, redox potential and spin transition energies were performed through DFT approximations for a series of Fe^{III}/Fe^{II} systems of the type [Fe(bztpen)OR]$^{2+/+}$ (R=Me, Et, *n*Pr, *n*Bu), which have a temperature dependent spin crossover behavior. These compounds exhibit changes in redox and magnetic properties, related to structural variations and are of importance for their possible applications among which signal generator materials stand out. Functionals B3LYP, ωB97X-D and TPSS along with PCM solvation model were evaluated for redox potential, while for spin crossover TPSSh functional was added. The multireference character of these compounds was also tested. Calculations were compared to experimental measurements, showing that ωB97X-D describes accurately the geometries observed in solid state for the low spin (LS) and high spin (HS) states and has the best correlation between calculated and experimental redox potential values. However, in the description of the spin transition energies the TPSS functional is needed to correctly describe the LS state as the observed ground state in the complexes at low temperature, this allows to calculate proper spin transition curves as a function of temperature. From these results, we obtained suitable approximations for an accurate description of redox potential and magnetic properties for the Fe^{III} coordination compounds, which can be extended to model similar systems.

Introduction

Spin crossover (SCO) behavior and redox properties in metal complexes are of interest because of their applications to several fields of chemistry such as biochemistry, catalysis, solar cells, energy storage devices, signal generator materials, among others. [1-6] These two properties can be modulated in some Fe^{III} / Fe^{II} compounds, by judicious modifications on the structure of the complexes produced.

In the field of SCO phenomena ligands of the Schiff base type provide one of the most versatile source of iron (III) SCO complexes. Typically, these complexes display a [Fe^{III}N$_4$O$_2$] coordination environment, which can be achieved by the participation of ancillary ligands [3].

Recently, we have studied the formation of [Fe^{II}(bztpen)X]$^{+/2+}$ complexes,[7] where bztpen is the nitrogen pentadentate ligand *N*-Benzyl-*N,N',N'-tris*(2-pyridylmethyl) ethylenediamine and X is an anion or solvent molecule (see Scheme 1a and 1b). The stability of these complexes in acetonitrile (CH$_3$CN) solution towards oxidation follows the expected spectrochemical series of the exogenous ligand X. In solid state, for halide and pseudo halide ligands X = Cl$^-$, Br$^-$, I$^-$, OCN$^-$ and SCN$^-$, resulting complexes are in a paramagnetic HS state, while the complexes are in diamagnetic LS state when X = [N(CN)$_2$]$^-$, CH$_3$CN, or CN$^-$. Two and one step SCO behaviors were observed in the solid state and in solution respectively for the dinuclear species [{Fe^{II}(bztpen)$_2$}{μ-N(CN)$_2$}](PF$_6$)$_3$.[8]

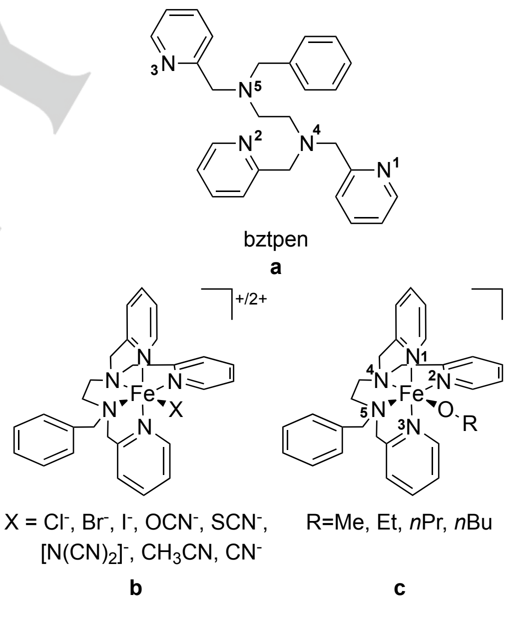

Scheme 1. **a**) Structure of the ligand *N*-Benzyl-*N,N',N'-tris*(2-pyridylmethyl)ethylenediamine (bztpen). **b**) Fe^{II} complexes [Fe(bztpen)X]$^{+/2+}$ (R= Cl$^-$, Br$^-$, I$^-$, OCN$^-$, SCN$^-$, [N(CN)$_2$]$^-$, CH$_3$CN, CN$^-$). **c**) Fe^{III} complexes [Fe(bztpen)OR]$^{2+}$ (R=Me, Et, *n*Pr, *n*Bu).

From these works, it could be inferred that the polypyridine-like bztpen ligand stabilizes the iron(II) ion reasonably well. However, in a later study we have observed that in the absence of coordinating species the Fe^{II}−bztpen system is unstable in methanol (MeOH) and other ROH solvents, giving rise to the stable species [Fe^{III}(bztpen)OR]$^{2+}$, where R = methyl (Me), ethyl (Et), *n*-propyl (*n*Pr) and *n*-butyl (*n*Bu) as in Scheme 1**c**.[9] The redox potential was measured in acetone for these complexes, and it was observed that none of these systems are reversible

---

[a] Facultad de Química (UNAM), Edificio B, Av. Universidad 3000, Coyoacán, Ciudad de México 04510. México.
E-mail: martham14@gmail.com, moresp@unam.mx, vmus@unam.mx, carlos.amador@unam.mx

Supporting information for this article is given via a link at the end of the document.

WILEY-VCH

and that the cathodic peak associated to a Fe^{III}/Fe^{II} reduction is the only one detected. This can be attributed to the instability of the $[Fe^{II}(bztpen)OR]^+$ complexes, implying that the value of redox potential obtained is only an approximation.

On the other hand, stable monometallic $[Fe^{III}(bztpen)OR]^{2+}$ complexes have a temperature dependent spin crossover behavior in solid state. The experimental observed arrangement of the compounds is in a pseudo-octahedral geometry and LS (S=1/2) to HS (S=5/2) transition is observed along with an increase of the metal–ligand (M−L) distances. Moreover, as the size of the substituent R is increased, an increase of the transition temperature ($T_{1/2}$) is observed, from 158 K for R=Me to 284 K for R=*n*Bu, suggesting a correlation between the size of the ligand and $T_{1/2}$.

From a theoretical point of view, an adequate description of these properties not only helps to understand the phenomena mentioned above but also helps to qualify the theoretical approaches that are used as tools in the design of new molecules with optimal properties. In this field density functional theory (DFT) has proven to have a good accuracy-cost relationship when dealing with relative large systems compared to wave function methods.

In this work, we evaluate magnetic and redox properties and their associated structural changes for the $[Fe(bztpen)OR]^{2+}$ series of complexes through several DFT approximations to get a suitable correlation between theory and experiment. We performed an accurate description of these properties, which can be extended to design new molecules of the same type whose properties could be optimized for the desired applications.

In the following section, we describe briefly the theoretical models employed to calculate the magnetic and redox properties. Subsequently results and discussion are presented.

Determination of redox and magnetic properties

In calculating the redox potential different methodologies have been reported. [10] A suitable one for metal complexes is based on the thermodynamic cycle shown in Figure 2, which has been used by several authors. [11-13]

$$\begin{tikzcd}
Ox_g + e^-_g \arrow[r, "\Delta G_g^{o,redox}"] \arrow[d, "\Delta G^o_{solv}\ (Ox)"'] & Red_g \arrow[d, "\Delta G^o_{solv}\ (Red)"] \\
Ox_s + e^-_s \arrow[r, "\Delta G_s^{o,redox}"'] & Red_s
\end{tikzcd}$$

Scheme 2. Born-Haber cycle used to estimate redox potentials.

According to this cycle, the standard Gibbs free energy of a redox half reaction in solution, $\Delta G_s^{o,redox}$, is obtained by calculating the change in free energy in gas phase, $\Delta G_g^{o,redox}$, and the solvation free energies of each of the species ΔG^o_{solv} (Red) and ΔG^o_{solv} (Ox), as shown in Equation 1.

$$\Delta G_s^{o,redox} = \Delta G_g^{o,redox} + \Delta G^o_{solv}(Red) - \Delta G^o_{solv}(Ox)\ \ldots\ (1)$$

Once $\Delta G_s^{o,redox}$ is obtained, the redox potential is calculated (E^o_{calc}) through the Nernst equation for the exchange of one electron (Equation 2).

$$\Delta G_s^{o,redox} = -FE^o_{calc}\ \ldots\ (2)$$

In order to obtain accurate redox potential (*E*) calculations the use of an internal reference system has been recommended to reduce the error between calculated and experimental values.[14] For metal complexes this internal reference corresponds to the ferrocenium/ferrocene (Fc^+/Fc) redox pair, which is also the system to be used experimentally recommended by the IUPAC.[15] Within the DFT approximations employed to calculate the redox potential, B3LYP has been one of the most widely used functionals,[11,13,14] however in a previous work other functionals such as ωB97X-D showed to provide more accurate results in the calculation of potential for the Fc^+/Fc system.[16]

For the SCO phenomenon, an energy diagram along one of the M−L coordinates can be used to describe the equilibrium between the LS and HS configurations for the octahedral Fe^{III} complexes, as shown in Figure 1. According to the diagram, since the minima are displaced both horizontally and vertically two main effects can be distinguished when a thermal transition LS→HS occurs. One is the change in the M−L bond distances (Δr_{HL}), which is a positive quantity if an increment from LS to HS is observed. The other is the change in energy from LS to HS (ΔE^0_{HL}), it can be seen that, the condition for thermal spin transition is that the zero-point energy difference between the two states should be positive and in the range of thermally accessible energies, $\Delta E^0_{HL} = E^0_{HS} - E^0_{LS} \sim k_BT$ (~2.47 kJ mol^{-1}).

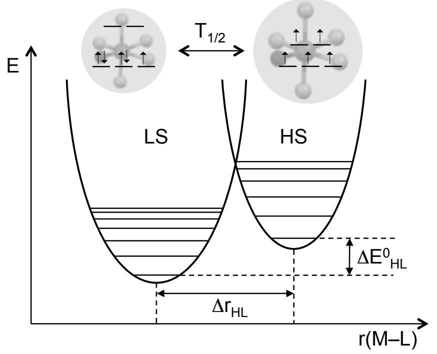

Figure 1. Energy diagram for the LS and HS states in the $[Fe(bztpen)OR]^{2+}$ complexes.

WILEY-VCH

Regarding the description of geometry, it is recognized that it is an important parameter because it is used to assess the quality of the approaches employed and also serves as a starting point for the description of the properties of interest. Several DFT functionals such as xDH-PBE0, PBE0, M06L and ωB97X have proved to perform accurately in the description of small and medium size organic molecules with deviations between 0.003−0.008 Å. [17] Nevertheless for molecules with transition metals, deviations increase with values from 0.020−0.400 Å as reported in the description of organometallic compounds of Ni, Pd, Ir and Rh,[18] where the hybrid functional B3LYP is one of the most used with relatively good performance. Additionally, the long-range functional ωB97X-D has been successful in the description of these metal complexes, probably due to the inclusion of dispersion interactions that are frequently present on this kind of systems. However, an adequate study of the SCO transition requires firstly an accurate description of the LS to HS geometry changes (Δr_{HL}) that can lead to a correct estimation of the spin transition energies (ΔE^0_{HL}). Once again, the B3LYP functional is one of the most widely used,[19] nevertheless the TPSSh hybrid functional has shown good results in particular for the calculation of ΔE^0_{HL} and also has been used in the determination of the spin transition curves.[20,21]

Results and Discussion

Redox Potentials

Redox potentials were measured in acetonitrile solution for the complexes $[Fe(bztpen)OR]^{2+}$ (R=Me, Et, *n*Pr, *n*Bu). Cyclic voltammetry (Figure 1) reveals an irreversible signal (E_{cp}) associated with the reduction from Fe^{III} to Fe^{II} for all the compounds with values from −0.310 to −0.278 V. This behavior is similar to the previously reported in acetone, [9] with an average shift of ~0.067 V toward positive values in acetonitrile.

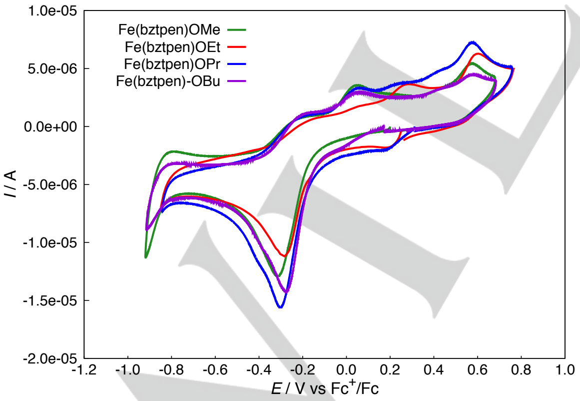

Figure 2. Cyclic voltammetry measured in CH_3CN (V vs Fc^+/Fc) for the $[Fe(bztpen)OR]^{2+}$ (R=Me, Et, *n*Pr, *n*Bu) complexes.

In order to confirm the cathodic peak associated to the reduction of Fe^{III} to Fe^{II} DFT calculations of the redox potential were performed with TPSS, B3LYP and ωB97X-D functionals, which were selected based in our previous calculations in the Fc^+/Fc^+ system.[16] The calculated redox potentials (E_{calc}) for the $[Fe^{III}(bztpen)OR]^{2+}$ referred to Fc^+/Fc are presented in Table 1 compared to the experimental E_{cp} values.

Table 1. Experimental and calculated redox potentials (V vs Fc^+/Fc) in CH_3CN for the $[Fe(bztpen)OR]^{2+}$ (R=Me, Et, *n*Pr, *n*Bu) complexes.

OR	E_{cp}	E_{calc}		
		TPSS	B3LYP	ωB97X-D
OMe	−0.310	−0.861	−0.500	−0.411
OEt	−0.283	−0.847	−0.464	−0.397
OPr	−0.303	−0.853	−0.492	−0.452
OBu	−0.278	−0.850	−0.429	−0.364

Experimentally, it seems that there is no significant effect of the substituent R on the potential, as they appear in values very close to each other. The functional that has the closest values to the experimental is ωB97X-D with the lowest mean absolute difference (MAD) of 0.113 V. Also for this functional it is possible to notice that calculated and experimental potentials do not appear in the same order, which is not surprising since the difference between them are below its precision. However, with these results, an adequate description of the redox potential for the reduction process from Fe^{III} to Fe^{II} is obtained.

To achieve a more accurate and quantitative description of this property we proceed to perform calculations of other iron systems to have a broader range on redox potential values in order to elaborate a correlation plot. Some of the Fe^{II}−bztpen previously mentioned were included; they have the formula $[Fe(bztpen)X]^{+/2+}$ (X=CH_3CN, NCO^-, CN^-), are reversible systems with experimental values reported in CH_3CN.[7] Moreover the structures of $Fe(Cp)_2$ and $Fe(Cp^*)_2$ (where Cp and Cp* are cyclopentadienyl and 1,2,3,4,5-pentamethylcyclopentadienyl ligands) were included. Experimental and calculated values are shown in Table 2, where the redox potential for the $[Fe(bztpen)OR]^{2+}$ (R=Me, Et, *n*Pr, *n*Bu) complexes was considered as an average since its values do not show dependence on the substituent R as mentioned above.

It is possible to notice that ωB97X-D remains the best functional with a MAD = 0.057 V, closest to the well known 0.058 V (at 298.15 K), which is the experimental difference between reduction and oxidation peaks for reversible systems that exchange one electron. [23] The correlation plot between calculated and experimental values is shown in Figure 3. The redox potentials for the $[Fe(bztpen)OR]^{2+}_{avg}$ are represented with their standard deviation bars in the graph. From the linear regression, correlation coefficients (R^2) were obtained, with

WILEY-VCH

values of 0.6751 for TPSS, 0.9381 for B3LYP and 0.9843 for ωB97X-D, which confirms the good performance of the latter functional in the description of this property.

Table 2. Experimental and calculated redox potentials (V vs Fc^+/Fc) in CH_3CN for Fe^{III} complexes $[Fe(bztpen)OR]^{2+}_{avg}$ and the Fe^{II} complexes $[Fe(bztpen)X]^{+/2+}$ (X=CH_3CN, NCO^-, CN^-), $Fe(Cp)_2$ and $Fe(Cp^*)_2$.

Compound	E_{exp}	E_{calc}		
		TPSS	B3LYP	ωB97X-D
$[Fe(bztpen)OR]^{2+}_{avg}$	−0.293	−0.853	−0.471	−0.406
$[Fe(bztpen)CH_3CN]^{2+}$	0.576	0.157	0.433	0.685
$[Fe(bztpen)NCO]^{+}$	0.145	−0.348	0.121	0.167
$[Fe(bztpen)CN]^{+}$	−0.074	−0.341	0.009	−0.014
$Fe(Cp^*)_2$	−0.539[a]	−0.649	−0.619	−0.536
$Fe(Cp)_2$	0.0[b]	0.025[b]	0.005[b]	0.035[b]
MAD	–	0.312	0.086	0.057

[a] Taken from reference 14. [b] Referred to 0.650 V from reference 22.

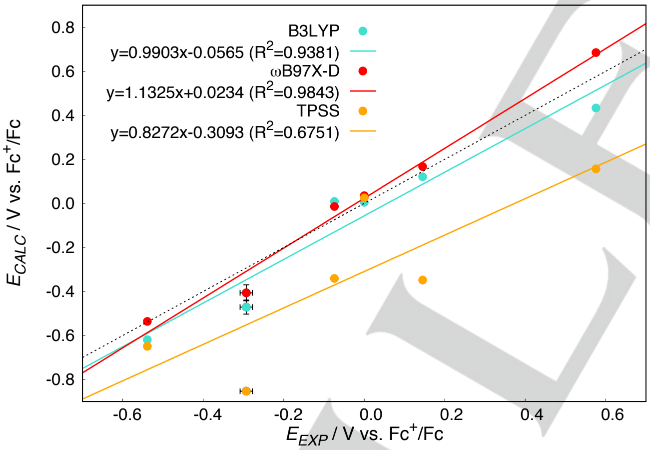

Figure 3. Correlation plot of the calculated and experimental redox potentials in CH_3CN (V vs Fc^+/Fc). For the $[Fe^{III}(bztpen)OR]^{2+}$ (R=Me, Et, *n*Pr, *n*Bu) complexes represented with an average value and its standard deviation bars. For the $[Fe^{II}(bztpen)X]^{+/2+}$ (X=CH_3CN, NCO^-, CN^-), $Fe(Cp^*)_2$ and $Fe(Cp)_2$ complexes represented with points.

Next, an analysis of the M-L bond distances in solution was performed to observe the change in geometry of alcoxide complexes $[Fe^{III}(bztpen)OR]^{2+}$ after reduction. The distances were obtained from fully optimized structures in CH_3CN with the ωB97X-D functional, not only for its performance in the description of the redox potential, but because as discussed in the next section also provides an accurate description of the bond distances for the LS and HS complexes.

For the $[Fe^{III}(bztpen)OMe]^{2+}$ complex it is possible to observe an increase in all M−L bond distances when an electron is added since $\Delta r(Fe^{III}\rightarrow Fe^{II})$ has positive values (see Table S1 for the M−L bond distances of all the complexes). This increase is particularly large in the Fe−O distance with a value of 0.117 Å, which can suggest the possibility of this bond being broken after reduction. This may help to explain the irreversibility observed in these systems, however, additional studies should be carried out in order to confirm such electrochemical behavior.

Table 3. M−L bond distances (Å) calculated with ωB97X-D in CH_3CN for $[Fe^{III/II}(bztpen)OR]^{2+/+}$ complexes.

Bond	$r(Fe^{III})$	$r(Fe^{II})$	$\Delta r(Fe^{III}\rightarrow Fe^{II})$
Fe−N(1)	2.107	2.200	0.092
Fe−N(2)	2.125	2.212	0.088
Fe−N(3)	2.160	2.227	0.066
Fe−N(4)	2.273	2.374	0.100
Fe−N(5)	2.251	2.353	0.102
Fe−O	1.782	1.900	0.117

Spin Crossover

As mentioned above, for the spin crossover an accurate description of structural and energetic changes (Δr_{HL} and ΔE^0_{HL}) associated to the process should be done. For this purpose a full optimization of the structures was performed in gas phase for the LS and HS states and results were compared to the experimental results reported by Ortega-Villar et al. [9] The same functionals that were used for the redox potentials were tested (TPSS, B3LYP and ωB97X-D), plus the hybrid TPSSh functional that was added for its good performance in the SCO description.

Experimentally for the $[Fe^{III}(bztpen)OR]^{2+}$ (R=Me, Et, *n*Pr, *n*Bu) complexes it is observed that at low temperature (100 K) the ground state configuration corresponds to LS, but when temperature is increased (300 K) the configuration corresponds to a HS state.

The change in M−L bond distances observed by X-Ray diffraction is an increment in the Fe−N bond lengths (numerated as in Scheme 1a), and a slight decrease in the Fe−O distance (See Tables S2-S5 for experimental and calculated values).

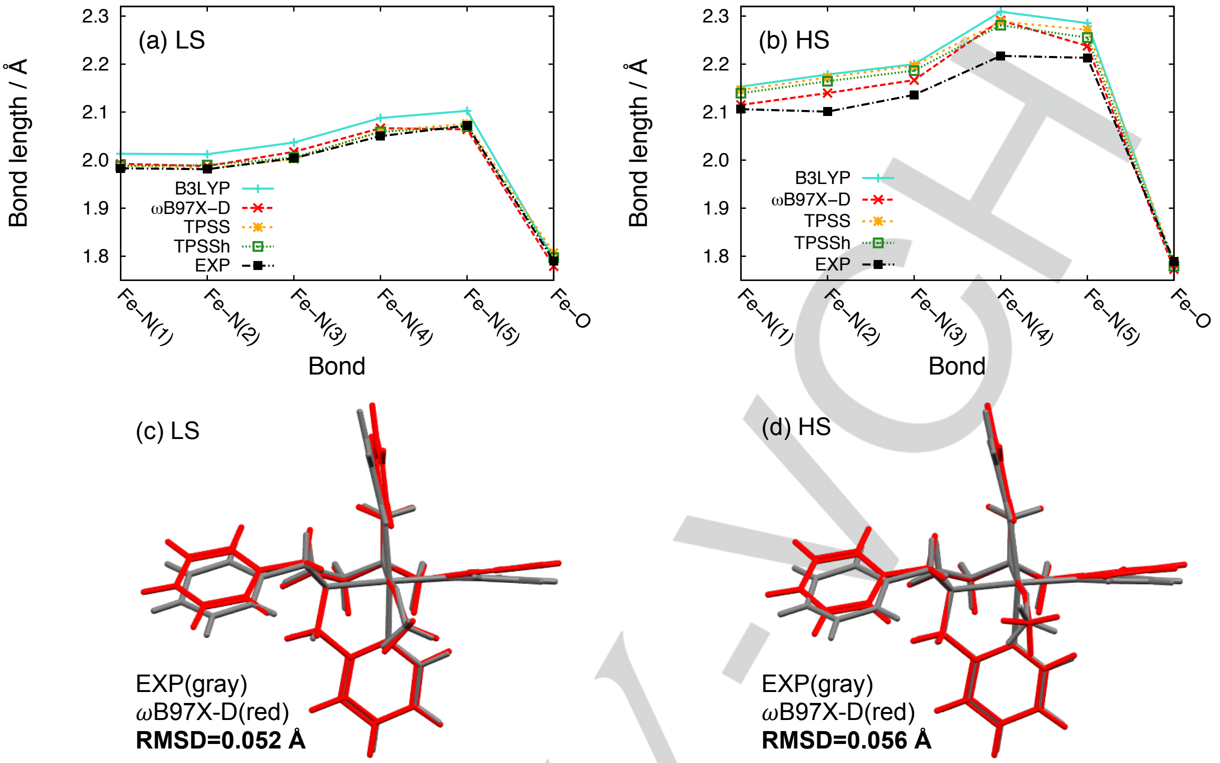

Figure 4. Calculated and experimental M−L bond lengths for the $[Fe^{III}(bztpen)OMe]^{2+}$ complex. (a) LS state calculated with B3LYP, ωB97X-D and TPSS compared with experimental structure at 100 K. (b) HS state calculated with B3LYP, ωB97X-D and TPSS compared with experimental structure at 300 K. (c) LS state structure overlap for the ωB97X-D and experimental (100 K) M−L bond lengths. (d) HS state structure overlap for the ωB97X-D and experimental (300 K) M−L bond lengths.

This increase in bond distances when moving from LS to HS can be observed in Figure 4a and 4b for the $[Fe^{III}(bztpen)OMe]^{2+}$ complex in black for the experimental values and colored for the different functionals. It is also reflected in the Δr_{HL} values presented in Table 4. In general, for the functionals tested it is observed that this trend is properly described in all cases for both spin states. However, among these functionals again ωB97X-D has the most accurate values in the description of this property as can be seen by the Δr_{HL}(calc) values in Table 4. This is also in agreement with the overlap between the experimental and calculated structures (considering only the M−L bond lengths for both spin states). We observed that ωB97X-D has the best fitting with an RMSD=0.052 Å for LS and RMSD=0.056 Å for HS as can be seen in Figures 4c and 4d, while B3LYP has RMSD=0.064 Å and 0.117 Å, TPSS has RMSD=0.072 Å and 0.122 Å and TPSSh has RMSD=0.075 Å and 0.112 Å for the LS and HS states respectively.

With this analysis, we can establish that any functional (among those tested), adequately predicts the geometries observed for the LS and HS states in the $[Fe^{III}(bztpen)OR]^{2+}$ (R=Me, Et, *n*Pr, *n*Bu) complexes. Furthermore, if a more precise description is required ωB97X-D has the best performance, where long-range separation and dispersion corrections seem to have an effect on the geometry description for these systems.

Table 4. Experimental and calculated Δr_{HL} (Å) for the $[Fe^{III}(bztpen)OMe]^{2+}$ complex (best results as compared to experiment in bold).

Bond	Δr_{HL} (exp)	Δr_{HL} (calc)			
		TPSS	TPSSh	B3LYP	ωB97X-D
Fe−N(1)	0.123	0.157	0.151	0.140	**0.123**
Fe−N(2)	0.120	0.189	0.175	0.166	**0.152**
Fe−N(3)	0.132	0.195	0.181	0.163	**0.149**
Fe−N(4)	0.167	0.228	0.222	**0.221**	0.224
Fe−N(5)	0.141	0.195	0.185	0.183	**0.174**
Fe−O	−0.001	−0.017	−0.018	−0.015	**−0.006**

In addition to the structural analysis, the spin transition energies (ΔE^{0}_{HL}) must be also adequately described. In Table 5, the experimental and calculated spin transition energies are presented for all the functionals tested.

WILEY-VCH

Table 5. Experimental and calculated spin transition energies ΔE^{0}_{HL} (kJ mol^{-1}) for the [Fe^{III}(bztpen)OR]$^{2+}$ (R=Me, Et, *n*Pr, *n*Bu) complexes.

OR	ΔE^{0}_{HL} (calc)			
	TPSS	TPSSh	B3LYP	ωB97X-D
OMe	17.229	−21.022	−36.127	−29.726
OEt	18.011	−20.067	−35.242	−34.160
OPr	17.685	−20.715	−36.072	−31.516
OBu	20.726	−16.945	−31.981	−30.479

It can be noticed that the only functional that correctly describes the LS state as the ground state is TPSS, which is a pure meta-GGA functional. All other functionals have negative transition energies and therefore invert the spin state, even ωB97X-D that had work properly for the redox potentials and geometries and TPSSh that has given good results in this type of calculations. In this case, the inclusion of a fraction of HF exchange seems to make unstable the LS configuration.

With an adequate description of the LS and HS states, provided by TPSS functional we proceeded to reproduce the experimental spin transition curves observed in the series of complexes. For this purpose, a methodology that has been used by some authors [20,21] is to treat the thermal spin crossover as a thermodynamic equilibrium between LS and HS states. The change in Gibbs free energy between these two states (ΔG_{HL}) at a certain temperature is related to the equilibrium constant ($K_{HL}=\gamma_{HS}/\gamma_{LS}$). Thus, the HS fraction (γ_{HS}) can be obtained by Equation 3.

$$\gamma_{HS} = \left[1 + e^{\Delta G_{HL}(T)/RT}\right]^{-1} \; \dots \; (3)$$

From the HS and LS fractions (γ_{HS} and γ_{LS}), calculated at a given temperature, the effective magnetic moment ($\mu_{eff}(T)$) can be estimated through Equation 4 and finally related to the temperature and magnetic susceptibility product ($\chi_M T$) through Equation 5.

$$\mu_{eff}(T) = \gamma_{HS}(T)\mu_{HS}(S_{HS}) + \gamma_{LS}(T)\mu_{LS}(S_{LS}) \dots \; (4)$$

$$\chi_M T = \left(\frac{\mu_{eff}(T)}{2.8278}\right)^2 \; \dots \; (5)$$

Performing a temperature scanning from 0 to 800 K for each of the complexes we calculate the $\chi_M T$ product and plot the values as function of temperature to obtain the spin transition curves. In Figure 5, the experimental and calculated spin transition curves are compared. It can be distinguished that the calculated spin transition curves (dashed lines) have the behavior expected for a transition from LS (S=1/2) to HS (S=5/2). However, there is a shift in the transition temperature ($T_{1/2}$) of about ~200 K between the calculated and experimental curves (See Table S6 for the actual values). Also, the trend of the increase in $T_{1/2}$ as a function of R substituent does not agree well with the experimental results.

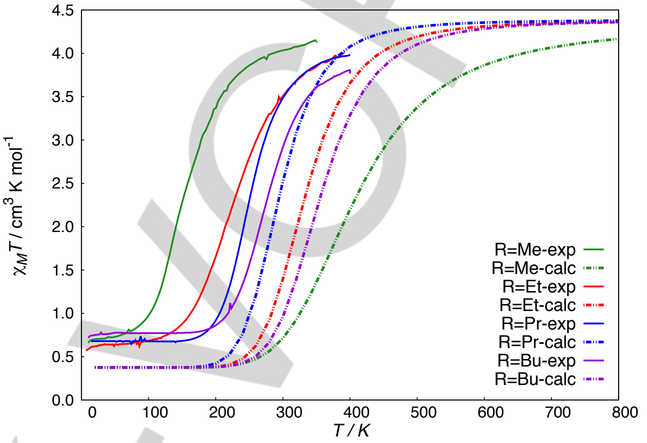

Figure 5. Spin transition curves for [Fe^{III}(bztpen)OR]$^{2+}$ (R=Me, Et, *n*Pr, *n*Bu) complexes experimental (solid lines) and calculated (dashed lines) with TPSS functional.

Despite this, the difference in temperatures between the calculated and experimental values is estimated around ~0.6 kcal mol^{-1}, which is acceptable for a theoretical calculation considering that chemical precision is estimated at ~1.0 kcal mol^{-1}. The small differences observed between R substituents remain as a challenge for DFT and the search for the universal functional.

Conclusions

In this work DFT calculations were performed of the redox potential, spin crossover phenomena and the structural changes observed in the Fe^{III} series of complexes of the type [Fe(bztpen)OR]$^{2+}$, where R=Me, Et, *n*Pr, *n*Bu. The functionals TPSS, B3LYP and ωB97X-D were tested for the redox potentials. For the SCO TPSSh functional was added.

It was found that ωB97X-D correctly describes the redox potential in Fe^{III}/Fe^{II} systems with a correlation coefficient R^2=0.9843. The geometry of the complexes is also well described for the LS and HS states with this functional with RMSD of 0.052 and 0.056 Å respectively.

For the SCO phenomena, according to the energy difference between low spin and high spin states, ΔE^{0}_{HL}, TPSS is the functional that describes the correct spin state (LS) at low temperature. With this functional it was possible to reproduce the spin transition curves, where a difference of ~200 K between the calculated and experimental curves is observed. However,

WILEY-VCH

this displacement (~0.6 kcal mol^{-1}) is within the order of what is considered chemical precision (~1.0 kcal mol^{-1}). To correctly reproduce the trend observed experimentally of the increase of $T_{1/2}$ as a function of R a greater precision of the functional is required.

Our results show that very different properties (redox potentials, minute structural changes and temperature dependent magnetic transitions), observed experimentally with the precision characteristic of each technique, can be described with reasonable accuracy by the current state of the art density functionals, providing further evidence that contributes to the understanding of the chemistry of these complex compounds. However, despite the good performance of the functionals for different properties, the existence of a universal functional that correctly describes all properties is still a challenge that is expected will be satisfied by further advances in the field of density functional theory.

Experimental Section

Compounds were obtained employing the synthesis reported by Ortega-Villar et al. [9] Potentiometric measurements for the $[Fe^{III}(bztpen)OR]^{2+}$ (R=Me, Et, *n*Pr, *n*Bu) complexes were performed in acetonitrile (CH_3CN) solution at room temperature with 0.1 M *N*-tetrabutylammonium hexafluorophosphate ($(C_4H_9)_4N(PF_6)$) as supporting electrolyte and υ=100 mV s^{-1}. CHInstrumets and Autolab PGSTAT 100 potentiostats were used. A system of three electrodes was employed, the working electrode being a glass carbon electrode, as reference electrode an Ag^+/Ag electrode in CH_3CN and a Pt-wire electrode as auxiliary electrode. Solutions were deoxygenated with N_2 and as recommended by IUPAC the Fc^+/Fc system was used as internal reference. Only the cathodic peak potential (E_{cp}) was considered to compare with E_{calc} values. Spin transition temperatures ($T_{1/2}$) were taken from the reported ones by Ortega-Villar et al. [9]

Computational details

All calculations were performed with Gaussian 09 package (C.01 and D.01 versions).[24,25] We evaluate the meta-GGA functional TPSS,[26] the hybrid functionals TPSSh[27] and B3LYP[28] and the long range corrected functional with dispersion corrections ωB97X-D.[29] The basis set used was a combination of SDD[30] for Fe atom and cc-pVTZ[31] for the rest of the atoms (C, H, O, N) denoted as SDD/cc-pVTZ. Solvent effects were considered through PCM [32] continuum model. All structures were optimized in gas phase and in acetonitrile (CH_3CN). With optimized geometries, free energies were computed via thermochemical analysis as implemented in Gaussian: at 298.15 K and 1 atm pressure for redox potential calculations making sure of no imaginary frequencies, while for the spin transition curves a temperature scanning from 0 to 800 K in steps of 20 K was performed in order to calculate the Gibbs free energies and obtain the magnetic susceptibility by temperature product ($\chi_M T$).

Acknowledgements

We acknowledge supercomputer services provided by DGTIC-UNAM (Miztli SC16-1-IG-37). M.M.F.-L. thanks CONACYT for financial support under scholarship number 240090. R.M.-E., V.M.U.-S. and C. A.-B. acknowledge support from FQ-PAIP.

Keywords: Redox potential • SCO behaviour • Chemical structure changes • Iron complexes • DFT calculations

[1] A. W. Munro, H. M. Girvan, K. J. McLean, *Nat. Prod. Rep.* **2007**, *24*, 585-609.
[2] P. G. Gildner, T. J. Colacot, *Organometallics* **2015**, *34*, 5497-5508.
[3] D. J. Harding, P. Harding, W. Phonsri, *Coord. Chem. Rev.* **2016**, *313*, 38-61.
[4] M. Grätzel, *J. Photochem. Photobiol., C* **2003**, *4*, 145-153.
[5] F. Pan, Q. Wang, *Molecules* **2015**, *20*, 20499-20517.
[6] K. Lin, Q. Chen, M. R. Gerhart, L. Tong, S. B. Kim, L. Eisenach, A. W. Valle, D. Hardee, R. G. Gordon, M. J. Aziz, M. P. Marshak, *Science* **2015**, *349*, 1529-1532.
[7] N. Ortega-Villar, V. M. Ugalde-Saldívar, M. C. Muñoz, L. A: Ortiz-Frade, J. G. Alvarado-Rodríguez, J. A. Real, R. Moreno-Esparza, *Inorg. Chem.* **2007**, *46*, 7285-7293.
[8] N. Ortega-Villar, A. L. Thompson, M. C. Muñoz, V. M. Ugalde-Saldívar, A. E. Goeta, R. Moreno-Esparza, J. A. Real, *Chem. Eur. J.* **2005**, *11*, 5721-5734.
[9] N. Ortega-Villar, A. Y. Guerrero-Estrada, L. Piñeiro-López, M. C. Muñoz, M. Flores-Álamo, R. Moreno-Esparza, J. A. Real, V. M. Ugalde-Saldívar, *Inorg. Chem.* **2015**, *54*, 3413-3421.
[10] K. Arumugam, U. Becker, *Minerals* **2014**, *4*, 345-387.
[11] L. E. Roy, E. Jakuvikova, M. G. Guthrie, E. R. Batista, *J. Phys. Chem.* **2009**, *24*, 6745-6750.
[12] M. Namazian, C. Y. Lin, M. L. Coote, *J. Chem. Theory Comput.* **2010**, *9*, 2721-2725.
[13] H. Kim, J. Park, Y. S. Lee, *J. Comput. Chem.* **2013**, *34*, 2233-2241.
[14] S. J. Konezny, M. D. Doherty, O. R. Luca, R. H. Crabtree, G. L. Soloveichik, V. S. Batista, *J. Phys. Chem. C* **2012**, *116*, 6349-6356.
[15] G. Gritzner, J. Kûta, *Pure Appl. Chem.* **1984**, *56*, 461-466.
[16] M. M. Flores-Leonar, R. Moreno-Esparza, V. M. Ugalde-Saldívar, C. Amador-Bedolla, *Comput. Theor. Chem.* **2017**, *1099C*, 167-173. http://dx.doi.org/10.1016/j.comptc.2016.11.
[17] E. Brémond, M. Savarese, N. Q. Su, A. J. Pérez-Jiménez, X. Xu, J. C. Sancho-García, C. Adamo, *J. Chem. Theory Comput.* **2016**, *12*, 459-465.
[18] T. Sperger, I. A. Sanhueza, I. Kalvet, F. Schoenebeck, *Chem. Rev.* **2015**, *115*, 9532-9586.
[19] H. Paulsen, V. Schünemann, J. A. Wolny, *Eur. J. Inorg. Chem.* **2013**, 628-641.
[20] M. Kaneko, S. Tokinobu, S. Nakashima, *Chem. Lett.* **2013**, *42*, 1432-1434.
[21] L. Piñeiro-López, N. Ortega-Villar, M. C. Muñoz, G. Mohlnár, J. Cirera, R. Moreno-Esparza, V. M. Ugalde-Saldívar, A. Bousseksou, E. Ruiz, J. A. Real, *Chem. Eur. J.* **2016**, *22*, 12741-12751.
[22] N. G. Connelly, W. E. Geiger, Chem. Rev. **1996**, *96*, 877-910.
[23] A. J. Bard, L. R. Faulkner in *Electrochemical Methods*: *Fundamental and Applications* (Eds.: D. Harris, E. Swain, C. Robey, E. Aiello), John Wiley & Sons, Inc., USA, **2001**.
[24] Gaussian 09, Revision C.01, M. J. Frisch, G. W. Trucks, H. B. Schlegel, G. E. Scuseria, M. A. Robb, J. R. Cheeseman, G. Scalmani, V. Barone, B. Mennucci, G. A. Petersson, H. Nakatsuji, M. Caricato, X. Li, H. P. Hratchian, A. F. Izmaylov, J. Bloino, G. Zheng, J. L. Sonnenberg, M. Hada, M. Ehara, K. Toyota, R. Fukuda, J. Hasegawa, M. Ishida, T. Nakajima, Y. Honda, O. Kitao, H. Nakai, T. Vreven, J. A. Montgomery, Jr., J. E. Peralta, F. Ogliaro, M. Bearpark, J. J. Heyd, E. Brothers, K. N. Kudin, V. N. Staroverov, T. Keith, R. Kobayashi, J. Normand, K. Raghavachari, A. Rendell, J. C. Burant, S. S. Iyengar, J. Tomasi, M. Cossi, N. Rega, J. M. Millam, M. Klene, J. E. Knox, J. B. Cross, V. Bakken, C. Adamo, J. Jaramillo, R. Gomperts, R. E. Stratmann, O.

WILEY-VCH

Yazyev, A. J. Austin, R. Cammi, C. Pomelli, J. W. Ochterski, R. L. Martin, K. Morokuma, V. G. Zakrzewski, G. A. Voth, P. Salvador, J. J. Dannenberg, S. Dapprich, A. D. Daniels, O. Farkas, J. B. Foresman, J. V. Ortiz, J. Cioslowski, and D. J. Fox, Gaussian, Inc., Wallingford CT, 2010.

[25] Gaussian 09, Revision D.01, M. J. Frisch, G. W. Trucks, H. B. Schlegel, G. E. Scuseria, M. A. Robb, J. R. Cheeseman, G. Scalmani, V. Barone, B. Mennucci, G. A. Petersson, H. Nakatsuji, M. Caricato, X. Li, H. P. Hratchian, A. F. Izmaylov, J. Bloino, G. Zheng, J. L. Sonnenberg, M. Hada, M. Ehara, K. Toyota, R. Fukuda, J. Hasegawa, M. Ishida, T. Nakajima, Y. Honda, O. Kitao, H. Nakai, T. Vreven, J. A. Montgomery, Jr., J. E. Peralta, F. Ogliaro, M. Bearpark, J. J. Heyd, E. Brothers, K. N. Kudin, V. N. Staroverov, T. Keith, R. Kobayashi, J. Normand, K. Raghavachari, A. Rendell, J. C. Burant, S. S. Iyengar, J. Tomasi, M. Cossi, N. Rega, J. M. Millam, M. Klene, J. E. Knox, J. B. Cross, V. Bakken, C. Adamo, J. Jaramillo, R. Gomperts, R. E. Stratmann, O. Yazyev, A. J. Austin, R. Cammi, C. Pomelli, J. W. Ochterski, R. L. Martin, K. Morokuma, V. G. Zakrzewski, G. A. Voth, P. Salvador, J. J. Dannenberg, S. Dapprich, A. D. Daniels, O. Farkas, J. B. Foresman, J. V. Ortiz, J. Cioslowski, and D. J. Fox, Gaussian, Inc., Wallingford CT, 2013.

[26] J. M. Tao, J. P. Perdew, V. N. Staroverov, G. E. Scuseria, *Phys. Rev. Lett.* **2003**, *91*, 146401.

[27] V. N. Staroverov, G. E. Scuseria, J. M. Tao, J. P. Perdew, *J. Chem. Phys.* **2003**, *119*, 12129-12137.

[28] A. D. Becke, *J. Chem. Phys.* **1993**, *98*, 5648-5652.

[29] J.-D. Chai, M. Head-Gordon, *J. Chem. Phys.* **2008**, *128*, 084106.

[30] M. Dolg, U. Wedig, H. Stoll, H. Preuss, *J. Chem. Phys.* **1987**, *86*, 866-872.

[31] T. H. Dunning, *J. Chem. Phys.* **1989**, *90*, 1007-1023.

[32] J. Tomasi, B. Mennucci, R. Cammi, *Chem. Rev.* **2005**, *105*, 2999-3093.

WILEY-VCH

Entry for the Table of Contents (Please choose one layout)

FULL PAPER

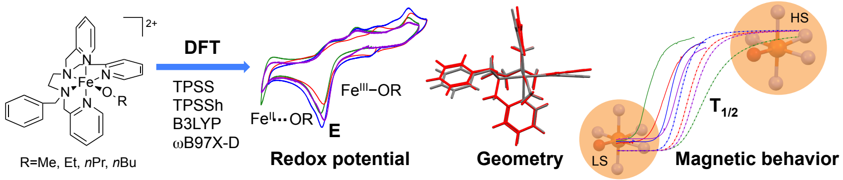

Different properties (redox potentials, minute structural changes and temperature dependent magnetic transitions), observed experimentally with the precision of each technique, can be described with reasonable accuracy by the current state of the art of DFT.

Martha M. Flores-Leonar[a], Rafael Moreno-Esparza[a], Víctor M. Ugalde-Saldívar[a], and Carlos Amador-Bedolla[a]*

Page No. – Page No.

Correlating properties in iron (III) complexes: A DFT description of structure, redox potential and spin crossover phenomena

WILEY-VCH

UNIVERSIDAD NACIONAL AUTÓNOMA DE MÉXICO

FACULTAD DE QUÍMICA

“EVALUACIÓN DE FUNCIONALES DE LA DENSIDAD EN EL ESTUDIO DE ESTRUCTURAS SUPRAMOLECULARES”

TESIS

QUE PARA OBTENER EL TÍTULO DE

QUÍMICA

PRESENTA

Nancy Cihuapilli Barrueta Flores

EXÁMENES PROFESIONALES
FACULTAD DE QUÍMICA

Ciudad Universitaria, Cd. Mx., 2016

JURADO

PRESIDENTE: **Dr. Jesús Valdés Martínez**

VOCAL: **Dr. Carlos Amador Bedolla**

SECRETARIO: **Dr. Luis Emilio Orgaz Baque**

1er. SUPLENTE: **Dr. Tomás Rocha Rinza**

2do. SUPLENTE: **Dr. Jorge Martín del Campo Ramírez**

Esta tesis fue desarrollada en:

Departamento de Física y Química Teórica
Entrepiso de la División de Estudios de Posgrado, Edificio B
Facultad de Química, Ciudad Universitaria.

Dr. Carlos Amador Bedolla
Asesor de Tesis

Nancy Cihuapilli Barrueta Flores
Sustentante

Agradecimientos

A la máxima casa de estudios, la Universidad Nacional Autónoma de México, por haberme permitido ser parte de ella y haberme preparado profesionalmente.

Al Dr. Carlos Amador Bedolla, por permitirme ser parte de su grupo de trabajo y contribuir en un proyecto muy grande y con un futuro prometedor. Gracias por la paciencia y confianza que me ha brindado.

A mis padres, por haberme hecho creer en un sueño, que ahora se hace realidad. Además del apoyo incondicional que siempre me han brindado.

A mi persona favorita, por ser mi complemento en la parte artística que yo no tengo, por darme la fuerza necesaria, por ser mi inspiración y un motivo más para seguir hacia adelante.

A toda mi maravillosa familia, que cree en mi y por la cual siento un cariño inmenso. Porque a pesar de los momentos difíciles que hemos vivido, siempre nos mantenemos unidos como muéganos.

A mis mejores amigos Thalia, Fer, Dora, Charly, Andrea, Bren, Abi, por formar parte de mi vida y por el apoyo que me dieron en todo momento, y que ahora se ve reflejado en la culminación de esta etapa.

A mis amigos del departamento de física y química teórica, Martha, Ger, Ro, Xiao, Jorge, Mirzam, por tener la paciencia para enseñarme cosas nuevas y por la diversión que hemos tenido juntos.

A mis amigos de la generación que contribuyeron en mi formación como química.

Al departamento de superación académica por los recursos y prestaciones otorgados a través del subprograma 127 "Formación básica en investigación".

A la Dirección General de Cómputo y de Tecnologías de Información y Comunicación por el tiempo de cómputo a través de la supercomputadora Miztli.

DETALLE DE USO

MARZO DE 2016

	INVESTIGADOR	NÚM. DE TRABAJOS	NÚM. HORAS NODO
1	CARLOS AMADOR BEDOLLA	9	4725.13
2	GERARDO ALVAREZ ALVAREZ	24	21245.75
3	MARTHA FLORES LEONAR	17	14402.1
4	PAULINO GUILLERMO CERON	65	2630.33
TOTAL		115	43003.31

ABRIL DE 2016

	INVESTIGADOR	NÚM. DE TRABAJOS	NÚM. HORAS NODO
1	CARLOS AMADOR BEDOLLA	15	8890.06
2	GERARDO ALVAREZ ALVAREZ	33	33579.64
3	MARTHA FLORES LEONAR	26	29275.19
4	PAULINO GUILLERMO CERON	65	16916.41
TOTAL		139	88661.3

MAYO DE 2016

	INVESTIGADOR	NÚM. DE TRABAJOS	NÚM. HORAS NODO
1	CARLOS AMADOR BEDOLLA	2	115.94
2	BRENDA CASANDRA VARGAS ROCHA	58	2442.84
3	GERARDO ALVAREZ ALVAREZ	8	16137.06
4	MARTHA FLORES LEONAR	17	24681.32
5	NANCY CIHUAPILLI BARRUETA FLORES	12	2495.86
6	PAULINO GUILLERMO CERON	94	4857.68

TOTAL		**191**	**50730.7**

JUNIO DE 2016

	INVESTIGADOR	NÚM. DE TRABAJOS	NÚM. HORAS NODO
1	BRENDA CASANDRA VARGAS ROCHA	108	6843.08
2	GERARDO ALVAREZ ALVAREZ	9	4024.52
3	MARTHA FLORES LEONAR	17	22207.05
4	NANCY CIHUAPILLI BARRUETA FLORES	4	1232.92
5	PAULINO GUILLERMO CERON	28	18385.2
TOTAL		166	52692.77

JULIO DE 2016

	INVESTIGADOR	NÚM. DE TRABAJOS	NÚM. HORAS NODO
1	CARLOS AMADOR BEDOLLA	8	1586.78
2	BRENDA CASANDRA VARGAS ROCHA	31	9041.83
3	MARTHA FLORES LEONAR	58	12112.88
4	NANCY CIHUAPILLI BARRUETA FLORES	18	6706.4
5	PAULINO GUILLERMO CERON	54	29688.04
TOTAL		169	59135.93

AGOSTO DE 2016

	INVESTIGADOR	NÚM. DE TRABAJOS	NÚM. HORAS NODO
1	CARLOS AMADOR BEDOLLA	36	6947.22
2	BRENDA CASANDRA VARGAS ROCHA	7	5303.82
3	GERARDO ALVAREZ ALVAREZ	22	16295.35
4	MARTHA FLORES LEONAR	43	21077.73
5	NANCY CIHUAPILLI BARRUETA FLORES	13	13587.01
6	PAULINO GUILLERMO CERON	42	22378.03
TOTAL		163	85589.16

SEPTIEMBRE DE 2016

	INVESTIGADOR	NÚM. DE TRABAJOS	NÚM. HORAS NODO
1	CARLOS AMADOR BEDOLLA	8	39.04
2	GERARDO ALVAREZ ALVAREZ	17	887.33

3	MARTHA FLORES LEONAR	32	14165.31
4	NANCY CIHUAPILLI BARRUETA FLORES	17	7101.78
5	PAULINO GUILLERMO CERON	87	53355.16
TOTAL		161	75548.62

OCTUBRE DE 2016

	INVESTIGADOR	NÚM. DE TRABAJOS	NÚM. HORAS NODO
1	GERARDO ALVAREZ ALVAREZ	12	4154.53
2	MARTHA FLORES LEONAR	56	14401.91
3	NANCY CIHUAPILLI BARRUETA FLORES	9	13472.4
4	PAULINO GUILLERMO CERON	58	24628.96
TOTAL		135	56657.8

NOVIEMBRE DE 2016

	INVESTIGADOR	NÚM. DE TRABAJOS	NÚM. HORAS NODO
1	GERARDO ALVAREZ ALVAREZ	20	16192.25
2	MARTHA FLORES LEONAR	97	20747.37
3	NANCY CIHUAPILLI BARRUETA FLORES	22	9053.16
4	PAULINO GUILLERMO CERON	29	16713.17
TOTAL		168	62705.95

DICIEMBRE DE 2016

	INVESTIGADOR	NÚM. DE TRABAJOS	NÚM. HORAS NODO
1	MARTHA FLORES LEONAR	69	27836.52
2	NANCY CIHUAPILLI BARRUETA FLORES	3	14153.96
3	PAULINO GUILLERMO CERON	27	19572.64
TOTAL		99	61563.12